J. Fluid Mech. (1976), *vol.* 78, *part* 4, *pp.* 785–819
Printed in Great Britain

On a turbulent 'spot' in a laminar boundary layer

By I. WYGNANSKI, M. SOKOLOV AND D. FRIEDMAN
School of Engineering, Tel-Aviv University, Ramat-Aviv, Israel

(Received 21 November 1975)

Artificially initiated turbulent spots in a Blasius boundary layer were investigated experimentally using hot-wire anemometers. Electrical discharges generated the spots, which grew in all directions as they were swept downstream by the mean flow. A typical lateral spread angle of the spots is 10° to each side of the plane of symmetry. Conditional sampling methods were used to form ensemble-averaged data yielding the average shape of a spot and the mean flow field in its vicinity. Far downstream a spot exhibits conical similarity and all quantities measured seem to be independent of the type of disturbance which generated the spot in the first place.

In plan view, the spot has an arrowhead shape whose leading interface is convected downstream somewhat more slowly than the free-stream velocity near the plane of symmetry and at approximately half the free-stream velocity at the extreme spanwise location. The trailing interface is convected at a constant velocity throughout ($U_{TE} = 0{\cdot}5\,U_\infty$). In this way the spot entrains laminar fluid through both interfaces, resulting in its elongation as it proceeds downstream. The flow near the surface accelerates abruptly as the leading interface passes by, however the acceleration continues within the spot and the velocity attains a maximum near the trailing interface. There is therefore a continuous increase in skin friction towards the trailing interface. Further away from the surface the passage of the spot is marked by deceleration followed by acceleration after the ridge of the spot passes the measuring station. All changes in velocity occur monotonically without causing inflexions or kinks in the ensemble-averaged velocity profiles. Although the displacement and momentum thicknesses change quite rapidly within the spot, the shape factor is practically constant in the interior region ($H = 1{\cdot}5$); and the velocity profiles may be very well represented by the universal logarithmic distribution. The spanwise velocity component W is everywhere directed outwards (i.e. away from the plane of symmetry) and increases with increasing z. The component of velocity normal to the surface is directed towards the plate near the leading interface and away from it in the remaining part of the spot.

Two-point velocity correlation measurements suggest that the spot may be represented by an arrowhead vortex tube which is convected downstream with a velocity equal to 65 % of the free-stream velocity. Fluid which is entrained near the plane of symmetry acquires a helical motion towards the extremities of the spot. This motion helps to explain the lateral as well as the longitudinal spread of the spot.

1. Introduction

The origin of turbulence in boundary-layer flow has attracted the interest of investigators for many years. The initial stages of boundary-layer instability are fairly well understood (Betchov & Criminale 1967), but our understanding wanes as the problem becomes progressively more complicated with the appearance of the finite amplitude three-dimensional disturbances which precede the breakdown to turbulence. The most thorough investigation into the mechanics of the phenomenon was done at the U.S. National Bureau of Standards (e.g. Klebanoff, Tidstrom & Sargent 1962), where the sequence of events leading to the birth of a turbulent spot was charted. Since the scope of this paper is limited to the turbulent spot itself we shall refrain from discussing these antecedent events here and the reader is directed to the review articles of Tani (1969) and Morkovin (1969).

The concept of turbulent spots created randomly as the boundary layer undergoes transition was originated by Emmons (1951) on the basis of visual observation in a water table. Emmons concluded that randomly generated spots grow uniformly and act independently of one another as they are swept downstream by the flow. He developed a model which related some statistical properties of the spots (e.g. their intermittency factor, burst frequency and period) to a single source-rate density function $g(x, y, t)$. Lacking experimental evidence, he assumed that g is a constant, suggesting that the spot production process may occur randomly throughout the boundary layer. Dhawan & Narasimha (1958) studied the intermittency factor for transition on a flat plate and concluded that Emmons's source density function could best be represented by a delta function (i.e. $g(x, y, t) = g\delta(x_t)$), implying that turbulent spots originate along a single line located at $x = x_t$. A recent report by Farabee, Casarella & DeMetz (1974) concurs with this general observation but points out that the intermittency factor is so insensitive to the choice of g that it should not be used as a criterion for the determination of the source density function. Farabee *et al.* suggested that the frequency of the bursts, and in particular, the point at which the frequency attains a maximum, may be used to define g. They then conclude that the source strength distribution is still not firmly established.

Elder (1962) investigated the conditions required for breakdown to turbulence and the degree of interaction between adjacent spots. A point-like breakdown, in which the spot originates from a very small volume within the boundary layer, was observed by him visually.

Kovasznay, Komoda & Vasudeva (1962) mapped the region of concentrated vorticity in a boundary layer prior to breakdown. The total length of the region in which the vorticity exceeds the value obtained in a Blasius boundary layer is approximately 4δ (δ is the boundary-layer thickness). Since the spot originates from within this region it may be surmised that breakdown to turbulence occurs essentially at a point. Elder also concluded that breakdown is determined by local conditions and is essentially independent of the Reynolds number and boundary-layer thickness. A critical Reynolds number is only required in order to amplify small disturbances, whereas sufficiently strong disturbances may

burst into turbulence almost instantaneously regardless of the Reynolds number. Thus the Reynolds number becomes merely an indicator for the amplification of natural disturbances rather than a criterion for the existence of turbulence. A velocity fluctuation with an intensity equivalent to 20 % of the free-stream velocity induced breakdown over the entire range of parameters investigated ($10^4 < Re_x \leqslant 10^6$, where Re_x is the Reynolds number based on distance from the leading edge). Another major assumption in Emmons's model, that the spots grow independently of one another even when they partly overlap, was verified by Elder. He observed the interaction between two artificially generated spots which were displaced laterally and concluded that there was no noticeable alteration in the growth rate of one spot owing to the presence of the other. This is a very significant finding in view of the suggestion that the bursts in a fully turbulent boundary layer are closely akin to the turbulent spots (Offen & Kline 1974; Coles & Barker 1974). Coles & Barker actually produced a synthetic turbulent boundary layer by generating regular arrays of spots. The degree of similarity between the synthetic and natural turbulent boundary layer remains to be demonstrated but the initial observations were encouraging.

The general shape of a turbulent spot, the angle at which it spreads and its propagation velocity while moving downstream were determined by Schubauer & Klebanoff (1956, henceforth referred to as S & K). There are, however, many loose ends yet to be tied together in order to establish the link between a perturbed laminar boundary layer and a fully developed turbulent flow. For example, the flow in the interior of a turbulent spot was not investigated and it would be interesting to know whether the spot contains all the elements of a fully turbulent boundary layer. If it does, this will easily explain the similarity between the synthetic boundary layer generated by Coles & Barker and the boundary layers occurring in nature. It will also indicate that we should probe the flow in more detail in order to isolate a more fundamental module which gives rise to the spot. The fact that the shape of the spot appears to be universally similar indicates that a higher degree of order is present in the spot than in the fully turbulent boundary layer. Similar questions have arisen in transitional flow in a pipe (Wygnanski & Champagne 1973). The turbulent slug already contains all the elements of a fully developed pipe flow and thus is too large a unit for a detailed investigation; on the other hand the puff bears no obvious similarity to turbulent pipe flow (Wygnanski, Sokolov & Friedman 1975). The link between the two flows is embedded in a complicated process of splitting which we are currently investigating but so far have not managed to isolate. We have begun to wonder whether the puff is not a freak of nature which is peculiar to pipe flow. We have thus decided to undertake the present investigation in order to look at the two flows simultaneously and try to establish some features which are common to both transition processes.

The experiment described here was performed at low speeds on a flat plate at $Re_x < 10^6$. Section 2 gives a complete description of the apparatus, while the data measuring systems and the manner in which the data was ensemble averaged are presented in § 3. The actual measurements of the flow field in the turbulent spot are discussed in § 4.

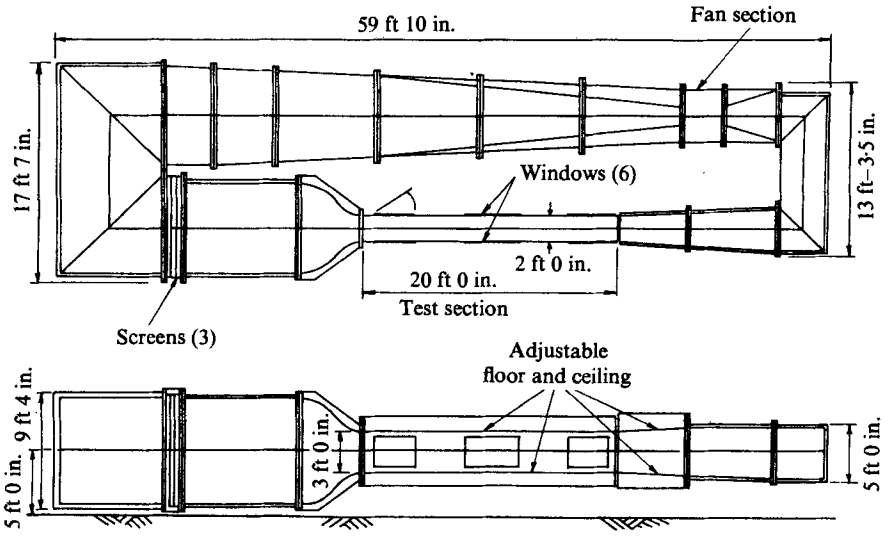

FIGURE 1. A schematic drawing of the wind tunnel.

2. Experimental apparatus

All measurements were made in a low speed, low turbulence, closed-circuit wind tunnel which was constructed by Kenney Engineering in Monrovia, California (figure 1). The test section is 2 ft wide, 20 ft long and nominally 3 ft high. The floor and ceiling of the test section are made of Plexiglas and are mounted on jacks, thus enabling the height of the section to be varied from 2 to 5 ft. The pressure gradient in the test section may be changed by the user according to the needs of the particular experiment. A 25 h.p. d.c. motor and a SCR controller provide a variable speed to a fixed-pitch-vane axial fan. The velocity in the test section can be varied from 0 to 45 m/s. The maximum deviation from the design velocity across the test section is less than 0·5 % outside the boundary-layer region. The longitudinal turbulence level is approximately 0·4 % at 30 m/s at a cross-section located 3 ft downstream of the inlet. For the present study an aluminium plate 12 ft long was mounted vertically in the tunnel. The upstream part of the plate was machined to include a wedge angle of 30°, which was later rounded off at the leading edge. The plate was positioned 3 in. from the tunnel wall and precautions were taken to eliminate the effects of the upstream boundary layer which exists on the wall of the wind tunnel. Irregularities in the surface of the plate were reduced by fastening the plate to the tunnel wall with adjustable spacers. The deviation of the plate from flatness was nowhere greater than 0·004 in. At the trailing edge an adjustable flap was installed in order to control the circulation about the plate and bring the stagnation point to the surface of interest. The possibility of giving a slight angle of attack to the whole plate and slightly diverging the top and bottom walls of the wind tunnel offered two additional degrees of freedom for the best adjustment of the pressure distribution along the plate. Corner fillets were added in order to reduce the influence of the top and bottom boundary layers. Static pressure measurements

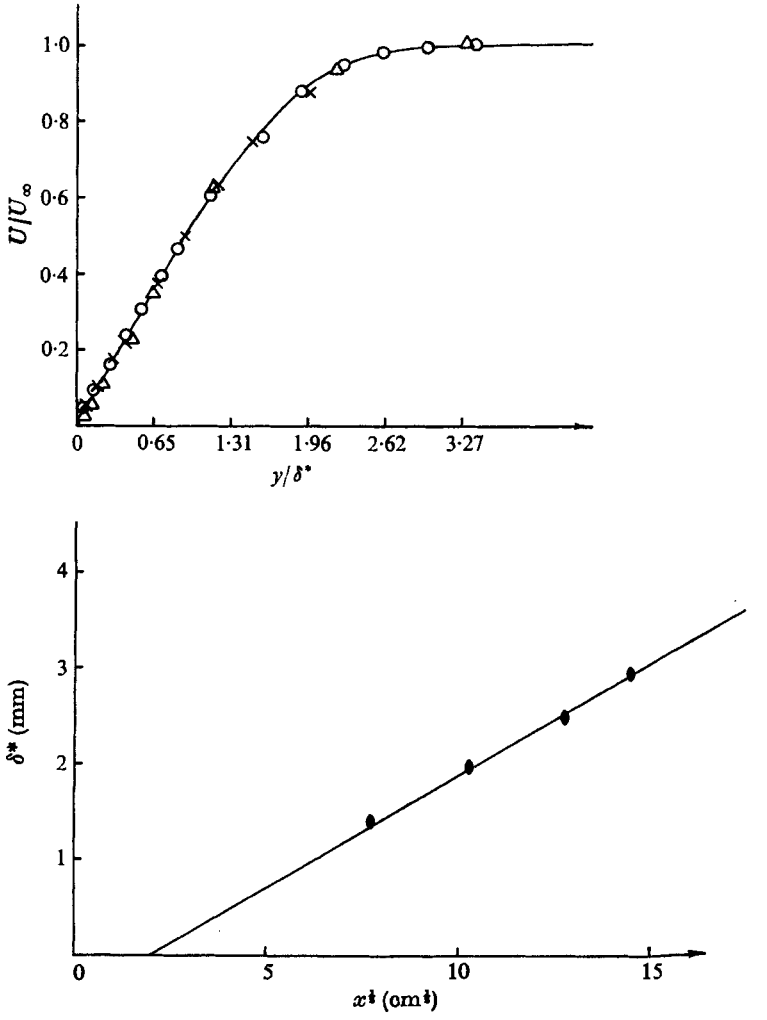

FIGURE 2. A laminar boundary-layer profile on the plate. $U_\infty = 8$ m/s. Distance x from plate in cm: O, 60; ×, 105; Δ, 163.

were made in order to show that the plate was nearly in a zero pressure gradient. The pressure field was fairly uniform and the maximum residual gradient in the region of the experiment was better than

$$\frac{1}{\frac{1}{2}\rho U_\infty^2}\frac{\Delta p}{\Delta x} = 3 \times 10^{-5}\,\mathrm{cm}^{-1}.$$

This dimensional pressure gradient is smaller than that in the investigation by Kovasznay *et al.* (1962).

The mean velocity profile was measured at three stations downstream of the leading edge and compared with the theoretical profile of Blasius (figure 2). The distance normal to the plate has been rendered dimensionless through division by δ^* (the displacement thickness). This is a much more definitive number than

δ (the boundary-layer thickness conventionally defined as the distance from the wall at which $U = 0{\cdot}99\,U_\infty$), which is prone to experimental errors as well as errors in interpretation. The variation of δ^* with distance from the leading edge is also shown in the figure. The results follows the law obtained from laminar boundary-layer theory. The hypothetical origin of the boundary layer is located 3·2 cm downstream of the leading edge of the plate.

Measurements were done with linearized constant-temperature DISA anemometers. Wires were calibrated in a wind tunnel or in a special calibration jet. The yaw sensitivity of the slanted wires was determined by direct calibration. Surveys were made of the longitudinal (U), normal (V) and spanwise (W) components of the mean velocity. Measurement of the spanwise component near the wall, which involves the use of two wires, was performed using a V-type arrangement in order to avoid difficulties arising from steep gradients across the layer. The separation between the centres of the wires in the V-probe was less than 1 mm. The distance between the wire and the plate were measured relative to zero as determined by an electric contact while the tunnel was running. The repeatability of this procedure is better than 0·02 mm.

The spark was generated by a capacitive discharge from a conventional electronic ignition unit which is often used in vehicles. The unit was triggered by a function generator and an electronic switch. The strength of the spark, its duration and its frequency of occurrence could all be altered but did not affect the results provided that sufficient time elapsed between consecutive events.

3. The measurement and processing of data

In order to obtain statistical data on the spot one would like to ensemble average the events. The simplest way of ensemble averaging the data is to trigger the instrumentation on the spark discharge itself and wait for the arrival of the spot at the measuring station. This is essentially the method by which Schubauer & Klebanoff (1956) obtained their data. Coles & Barker (1974) and Komoda (1974, private communication), who are working on similar aspects of the problem, proceeded in the same way. By using the disturbance to trigger the measurement system one implicitly assumes that the spot is convected downstream at a constant speed and that its size and shape are identical for all the events. This assumption is fairly good if one is only interested in the gross characteristics of the spot. If one desires to learn more about the flow near the interface, the ensemble averaging of data must be more precise since the velocity of propagation and the shape of the spot vary slightly from event to event. This variation tends to smear out the sharpness of the interface which is visible for each individual event. For this reason we have invested considerable effort in perfecting the measurement and processing of the data, a detailed description of which follows.

All data processing was done digitally, using a system consisting of a small computer (Varian 620/i) with 16384 words of 16-bit memory, 7-track digital magnetic tape and analog-to-digital conversion equipment of 12-bit precision (4096 quantizing steps). Data were recorded using three probes, here labelled

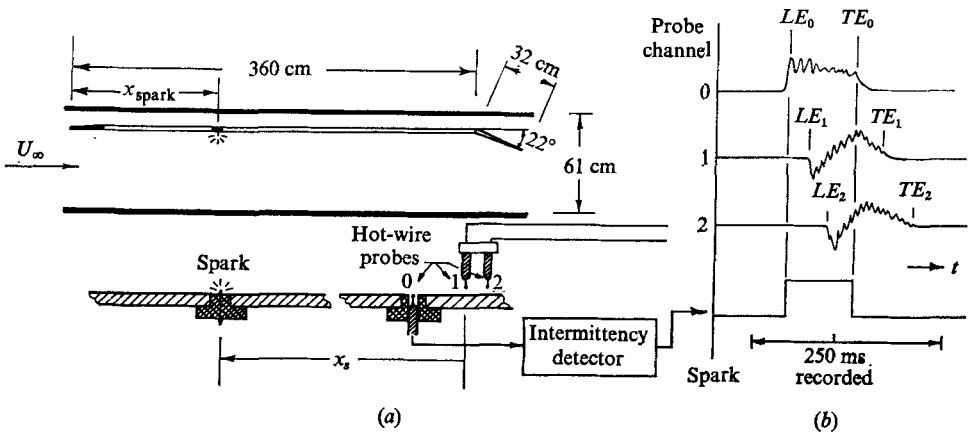

FIGURE 3. (*a*) The layout of the experiment and (*b*) a schematic drawing showing the acquisition of data.

0, 1 and 2 (see figure 3). Probe 0 was fixed flush with the surface of the plate, and served for time-synchronization only; the signal was fed to an intermittency detector which produced a square pulse as the spot passed over the probe. Probes 1 and 2 were mounted in the air stream with probe 2 at a known distance downstream of probe 1.

The time relationships of the resulting signals are shown in figure 3(*b*), with leading- and trailing-edge passage times indicated by LE_0, etc. For each occurrence of a spot, the three data channels were digitized for 250 ms at a rate of 10000 samples/s per channel, starting at a predetermined time after the triggering spark. (Channels 1 and 2 were low-pass filtered at 4 kHz to avoid aliasing effects.) The skew time between samples from adjacent channels was 10 μs.

The information to be derived from the digitized wave forms was the following:

(i) Leading- and trailing-edge time differences between the probes to allow the shape of the spot to be mapped.

(ii) Averaged wave forms from channel 1, for plotting velocity profiles and streamlines.

Early in the experimental work it was found that the spot wave shape varied somewhat in amplitude and duration from one realization to another, and in many cases (especially at locations relatively far from the plate) the leading and trailing edges were not distinct. For these reasons the first step in processing was to develop a criterion for locating the leading and trailing edge of each spot individually, so that these times could be averaged and identified with a particular point on the spot.

Visual location of the interface using a digital display was considered; however this was finally ruled out by the total time required for processing a sufficient quantity of data to get reasonably accurate averages. The final procedure involved a frequency filtering operation yielding the envelope of the turbulent fluctuation component of each individual spot. This was compared with a fixed threshold level to obtain the leading- and trailing-edge times.

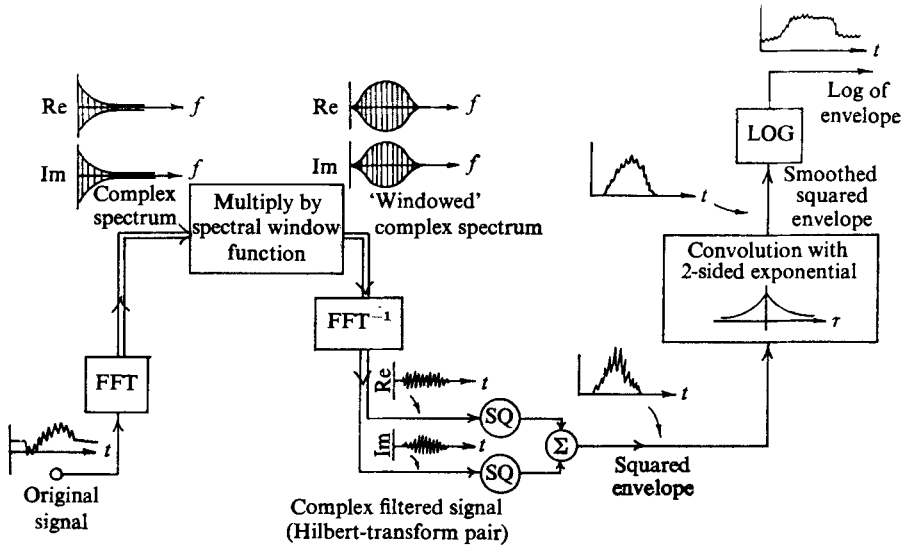

FIGURE 4. A schematic representation of the filtering procedure.

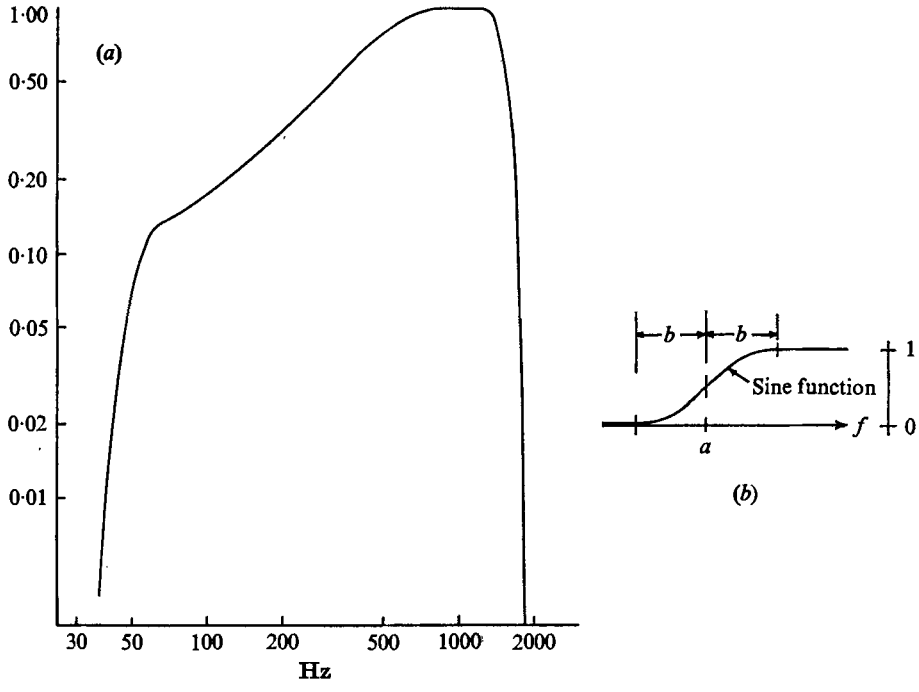

FIGURE 5. The window function used in the filtering procedure.

The filtering procedure is shown schematically in figure 4. A fast Fourier transform program was used to obtain the complex spectrum of the given wave form, located within a time interval of 204·8 ms (2^{11} samples). The spectrum was then multiplied point by point by a 'spectrum window' function, which combined the desired band-pass with a frequency weighting factor favouring the higher

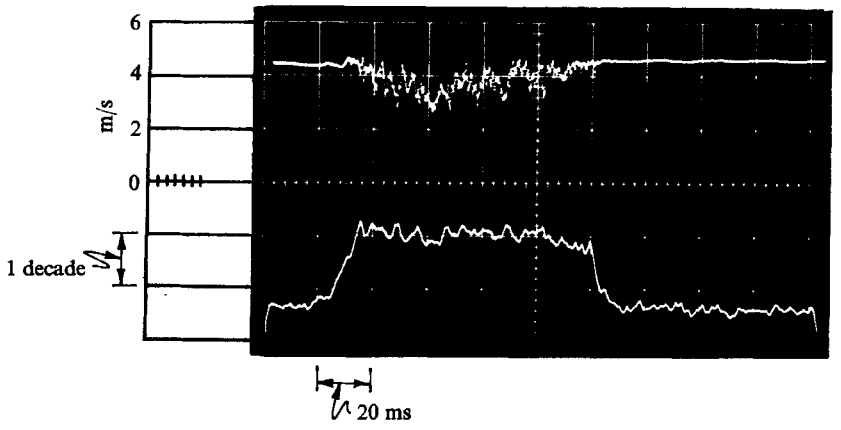

FIGURE 6. An oscillogram showing a typical streamwise velocity trace in a spot and a processed wave form for the detection of turbulence.

frequencies. Figure 5(*a*) shows the window function used. The window function was chosen as the product of three factors each of form

$$\begin{aligned} \tfrac{1}{2}\{1+\sin[\tfrac{1}{2}\pi(f-a)/b]\} \quad &\text{for} \quad -1 \leqslant (f-a)/b \leqslant 1, \\ 0 \quad &\text{for} \quad (f-a)/b < -1, \\ 1 \quad &\text{for} \quad (f-a)/b > 1, \end{aligned}$$

shown on linear scales in figure 5(*b*), where a and b were chosen as follows:†

	a	b
(1)	48·8 Hz	14·6 Hz (high pass),
(2)	312·5 Hz	468·8 Hz (weighting),
(3)	1563 Hz	−312·5 Hz (low pass).

The object here was not to preserve the frequency content of the turbulent spectrum, but rather to emphasize the region which would give the best discrimination between turbulent and laminar flow. It was found that frequencies above 500 Hz are most useful for this purpose, although their contribution to the total turbulent energy is relatively small. Note also that this method of filtering (FFT, windowing and inverse FFT) introduces no phase-shift distortion.

The windowed complex spectrum was transformed back in such a way as to give a complex function in time, i.e. two signals derived from the original. These signals have the property of being Hilbert transforms of one another; every frequency component in one appears in the other with the same amplitude but displaced by 90° in phase. Squaring them individually and then summing gives the square of the true envelope of the filtered signal.

The squared envelope was smoothed by convolution with a double-sided exponential impulse response of the form $\exp(-|\tau|a)$, with τ representing time and $a = 0{\cdot}8$ ms, and the logarithm taken. Use of the logarithmic scale for the final envelope has two justifications: to make signal activity apparent over the

† These specific values were chosen for convenience in octal representation in the processing program and are not critical in any way.

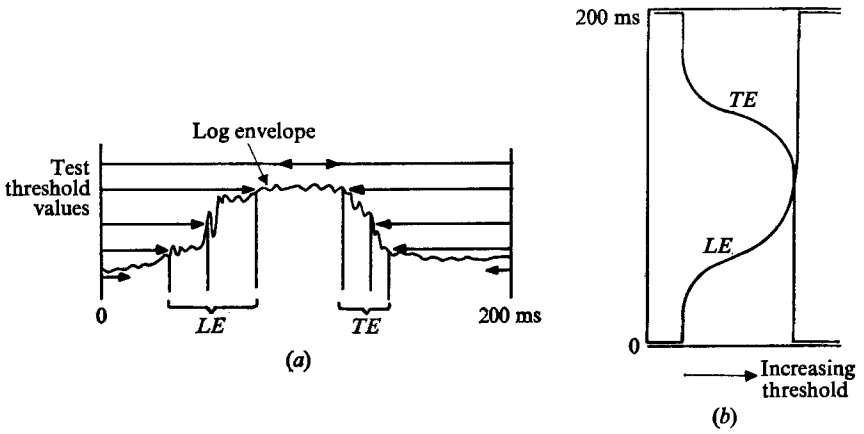

FIGURE 7. Leading- and trailing-edge times as a function of threshold.

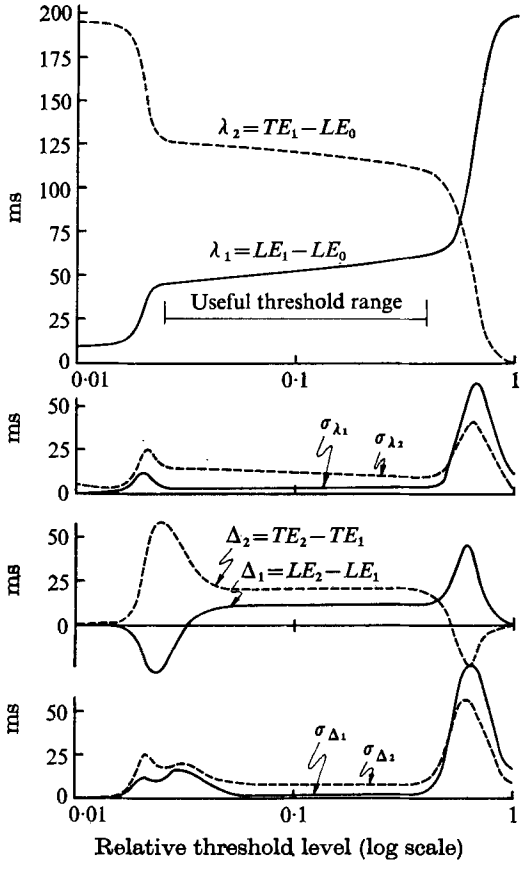

FIGURE 8. The detection of the leading and trailing interfaces and their propagation velocity as a function threshold level. Station 305; 118 events averaged.

entire dynamic range and to allow the threshold level to be expressed on an amplitude ratio scale. Typical wave forms (for channel 1) are shown in figure 6. Note that the leading and trailing edges of the spot are indistinct in the probe signal, while the envelope resembles a trapezoidal pulse with definite rise and fall.

The interface passage times are defined by the points at which the envelope wave form crosses a specified threshold level. For this purpose it must first be determined whether a range of suitable levels in fact exists, in view of the variations in amplitude among observed spots. To answer this question, a program was written to give average times for LE_1, TE_1, LE_2 and TE_2 relative to LE_0 (figure 3*b*) *as functions of the threshold level* over a range of approximately 2·5 decades of input amplitude. Leading edges were defined by searching forwards in time until a sample point of the logarithmic envelope was found which exceeded the threshold, and similarly for the trailing edges by searching backwards, as shown in figure 7(*a*). This gives two functions of the threshold level, labelled LE and TE in figure 7(*b*), which were then averaged over many individual spots recorded at a given station. A typical output is shown in figure 8: the averaged times $\lambda_1 = LE_1 - LE_0$, $\lambda_2 = TE_1 - LE_0$, $\Delta_1 = LE_2 - LE_1$ and $\Delta_2 = TE_2 - TE_1$ and their standard deviations are plotted as functions of threshold over a range of two decades. Note that a region of low slope and small standard deviation does exist, and is indicated in the figure as the useful threshold range. A suitable level may be chosen for all spots and the averaged times read from the plot. Averaged velocities were obtained from the leading hot-wire probe (labelled as probe 1 in figure 3*a*). The averages were generated by determining the position of the leading and trailing front for each spot and aligning the hot-wire traces of all events at either edge. In this way two separate ensemble averages were obtained: one triggered by the leading edge and one triggered by the trailing edge. These results show more detail near the respective interfaces than single ensemble averages because variations in time of occurrence or spot length do not affect the result in the vicinity of the triggering point.

4. Results and discussion

The shape of the spot and its velocity of propagation

It is important to establish that the spot which we have investigated is a universal structure in a laminar boundary layer. It is also important to establish the adequacy of our interface discrimination. For this purpose a typical spot may be drawn in a t, y, z co-ordinate system because it is obtained directly from the averaged times λ_1 and λ_2 in figure 8, where t represents time rather than longitudinal distance.†

A cross-section of the spot through its plane of symmetry is marked by a dashed line in figure 9(*a*). It has a triangular shape with rounded corners. The leading interface has a slight overhang, which is most advanced at an elevation of about a quarter of the height of the spot. The trailing interface is quite blunt near the wall. Coles & Barker (1974) obtained the shape of the spot from ensemble-

† 'Normalized time' is a dimensionless quantity obtained through division of all time intervals by the time which it takes the spot to pass the measuring station at $y = z = 0$.

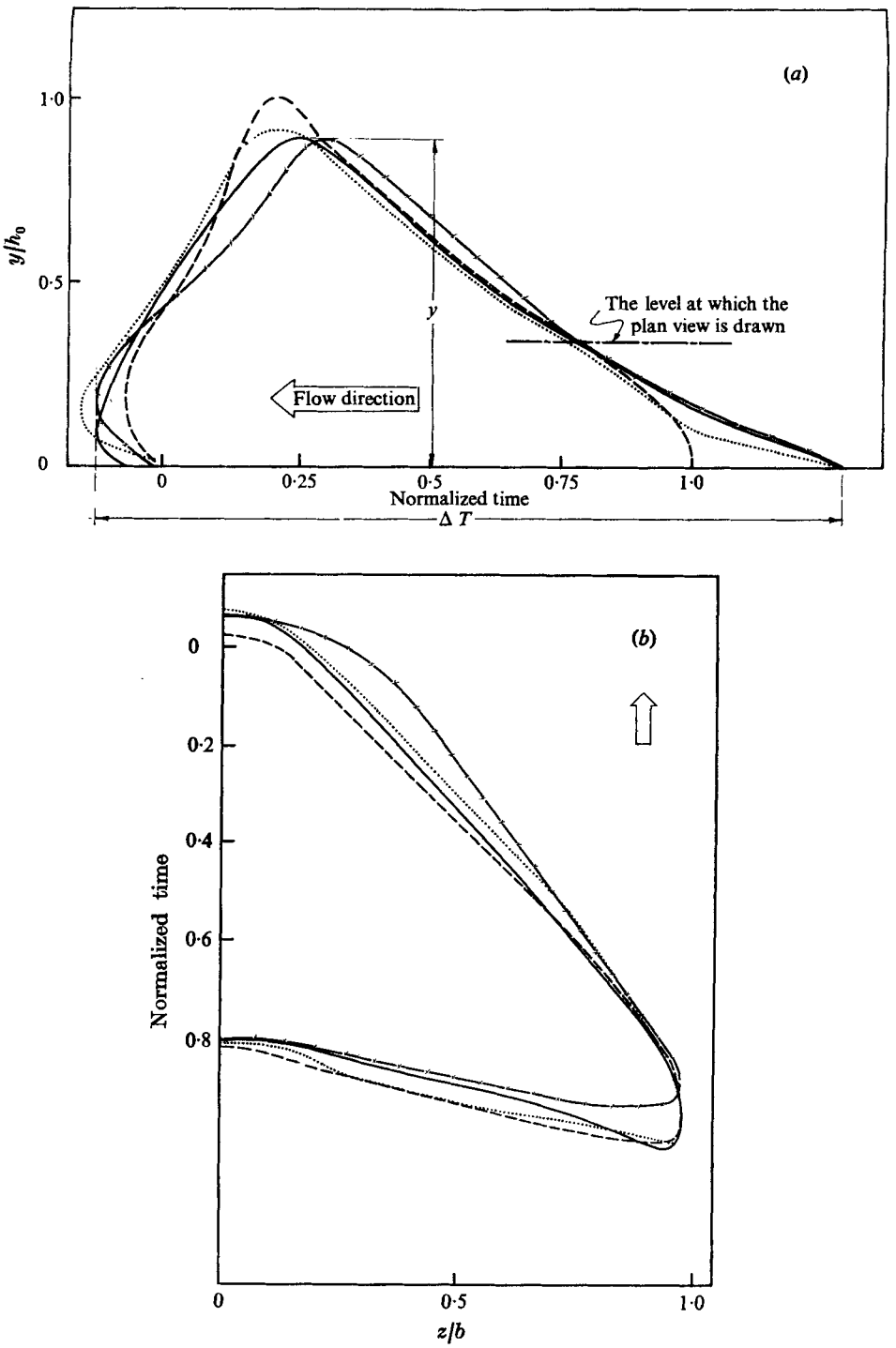

FIGURE 9. Two cross-sections through a spot: a comparison of criteria. $U_\infty = 9{\cdot}4$ m/s. (*a*) Elevation. (*b*) Plan. —×—, Coles & Barker (1974); – – –, our criterion. Shape based on 2% deviation in U: · · · · ·, LE ensemble average; ——, TE ensemble-averaged.

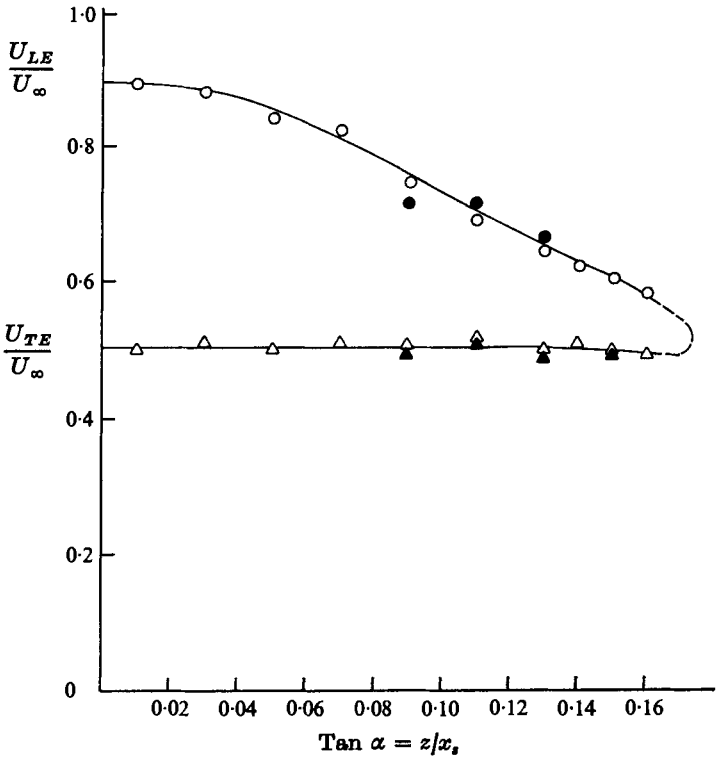

FIGURE 10. The spanwise variation of the propagation velocities of the spot. ○, U_{LE}/U_∞, $y = 5$ mm; △, U_{TE}/U_∞, $y = 5$ mm; ●, U_{LE}/U_∞, $y = 0{\cdot}4$ mm; ▲, U_{TE}/U_∞, $y = 0{\cdot}4$ mm.

averaged velocities which were conditioned to their disturbance generator. They defined the boundaries of the spot as the locus of points at which the velocities deviated by 2 % from the free-stream value. We adopted an identical procedure and compared the two shapes by equating the maximum time span Δt and height y in the two experiments. For the purpose of comparison the trailing-edge ensemble-averaged velocities were used.

The differences in shape between Coles & Barker's results and ours (using their criterion) are not very large. They are of the same order of magnitude as the differences between our LE-ensemble-averaged data and our TE-ensemble-averaged data, where LE and TE stand for leading and trailing edge respectively. The discrepancies can easily be attributed to the fact that Coles & Barker ensemble averaged their velocities relative to the disturbance generator. The major difference between our criterion for the boundaries of the spot and theirs is apparent at the extremities, where the maximum difference in length at the surface amounts to 25 % of the total length of the spot. This difference is caused by the velocity field which the spot induces outside its boundaries. For example, the velocity near the surface rises quite abruptly as the spot arrives at the wire but falls very slowly after it has left (see figure 16 or figure 6 in S & K). Since the rise in velocity is abrupt at the leading edge the two criteria agree very well at this point; however, the slow exponential-like decay of velocity near the

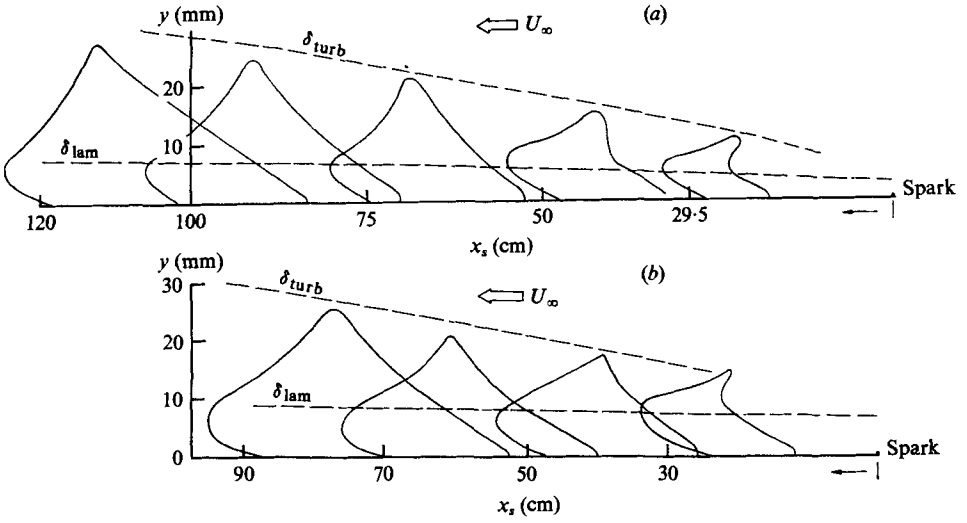

FIGURE 11. The development of the spot along the plane of symmetry. (*a*) $x_{spark} = 30$. (*b*) $x_{spark} = 90$.

surface after the trailing edge contributes to the large discrepancy between the two viewpoints.

The plan view of the spot in this co-ordinate system is shown in figure 9(*b*). The relative elevation at which the plan view is drawn was picked by Coles & Barker and we have adopted it for the sake of comparison. The difference between the two criteria at this elevation is negligible. However, Coles & Barker's spot has a slightly blunter leading edge near the plane of symmetry. If we assume that the leading interface is convected downstream with velocity U_{LE} equal to the free-stream velocity, we find that the leading edge of the spot is swept backwards at $\theta = 15{\cdot}2°$. This agrees remarkably well with the findings of S & K.

The shape of the spot can be transformed to a laboratory co-ordinate system if the propagation velocity of each interface is known. These velocities can be obtained from the time intervals Δ_1 and Δ_2 shown in figure 8, i.e. from the time it takes for the interface to move from probe 1 to probe 2 (figure 3). In order to obtain the propagation velocity locally one would like to place the hot-wire probes close to one another. However, even if one overcomes the wake interference problem the accuracy of the measurement decreases with decreasing separation between the probes because the shape of the spot is not really frozen, neither is the interface smooth (see Elder's photographs). There is always the danger that two wires separated by a small distance will be sensitive to fluctuations in the shape of the interface rather than its overall velocity. We experimented with the spacing between the probes, varying their separation from 2 to 30 cm, and decided on 10 cm as a reasonable compromise.

The probes were initially placed one directly behind the other, and interference was avoided by making the leading wire longer than the rear wire. Nevertheless nonsensical results were obtained at large spanwise locations, which indicated that the velocity of the leading interface increased with increasing z. Propagation velocities three times larger than the free-stream

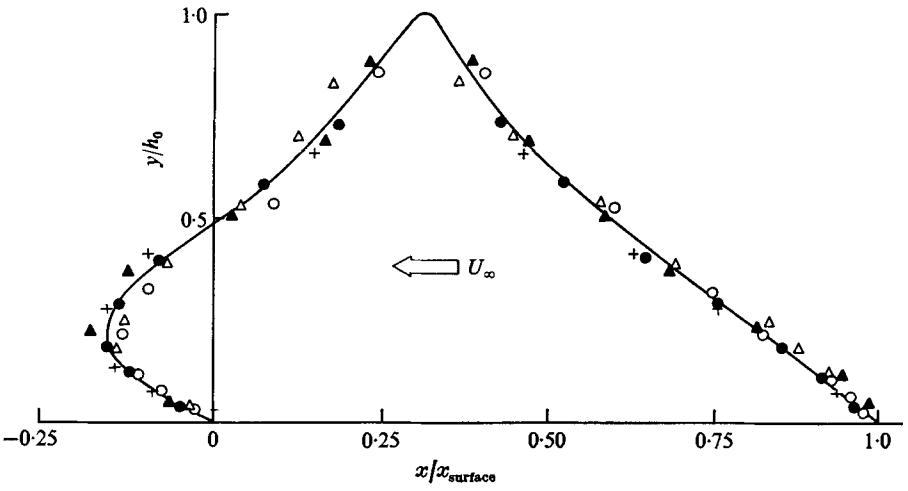

FIGURE 12. A normalized elevation view of five different spots.

	▲	○	△	+	●
x_s	75	100	120	70	90
x_{spark}	30	30	30	90	90

velocity were recorded. Since it was observed that the spot grows linearly with distance x_s from the point of breakdown (i.e. spark), we tried locating the wires on rays emanating from the spark, ensuring that the measurements were made at the same spanwise location of the spot. The results are shown in figure 10. The propagation velocity U_{TE} of the trailing edge is $0{\cdot}5\,U_\infty$ and seems to be independent of the co-ordinates x, y and z; the propagation velocity U_{LE} of the leading edge is $0{\cdot}89\,U_\infty$ on the plane of symmetry only and decreases slowly with increasing z. These observations are in agreement with S & K's results on the surface of the plate. We did not observe, however, an increase in U_{LE} with y. It is plausible that U_{LE} does not actually increase with y but only appears to do so owing to the spread of the spot in the y direction. This effect corresponds to our initial measurement of U_{LE} at different spanwise locations and would be most evident for large distances between the measuring stations. Only two such values of y are indicated in figure 10; however, we have made similar measurements at numerous values of y, particularly near the plane of symmetry.

Elevation views of developing spots are shown in figures 11 (*a*) and (*b*). In figure 11 (*a*) the spark was located 30 cm from the leading edge while in figure 11 (*b*) it was placed 90 cm further downstream, the free-stream velocity being maintained at 9·4 m/s in both cases. The Reynolds numbers Re_{δ^*} based on the laminar boundary-layer displacement thickness at the spark were 508 and 1220 respectively. The shape of the spot was deduced from time records obtained at various distances from the spark and the convection velocities of the respective interfaces. The numbers shown on the abscissa indicate the average distance of the leading interface from the spark, integrated over the height of the spot and ensemble averaged with respect to the number of events. It appears that in both cases the spot attains a characteristic terminal shape approximately 70 cm downstream of the disturbance. The height of the overhang of the leading

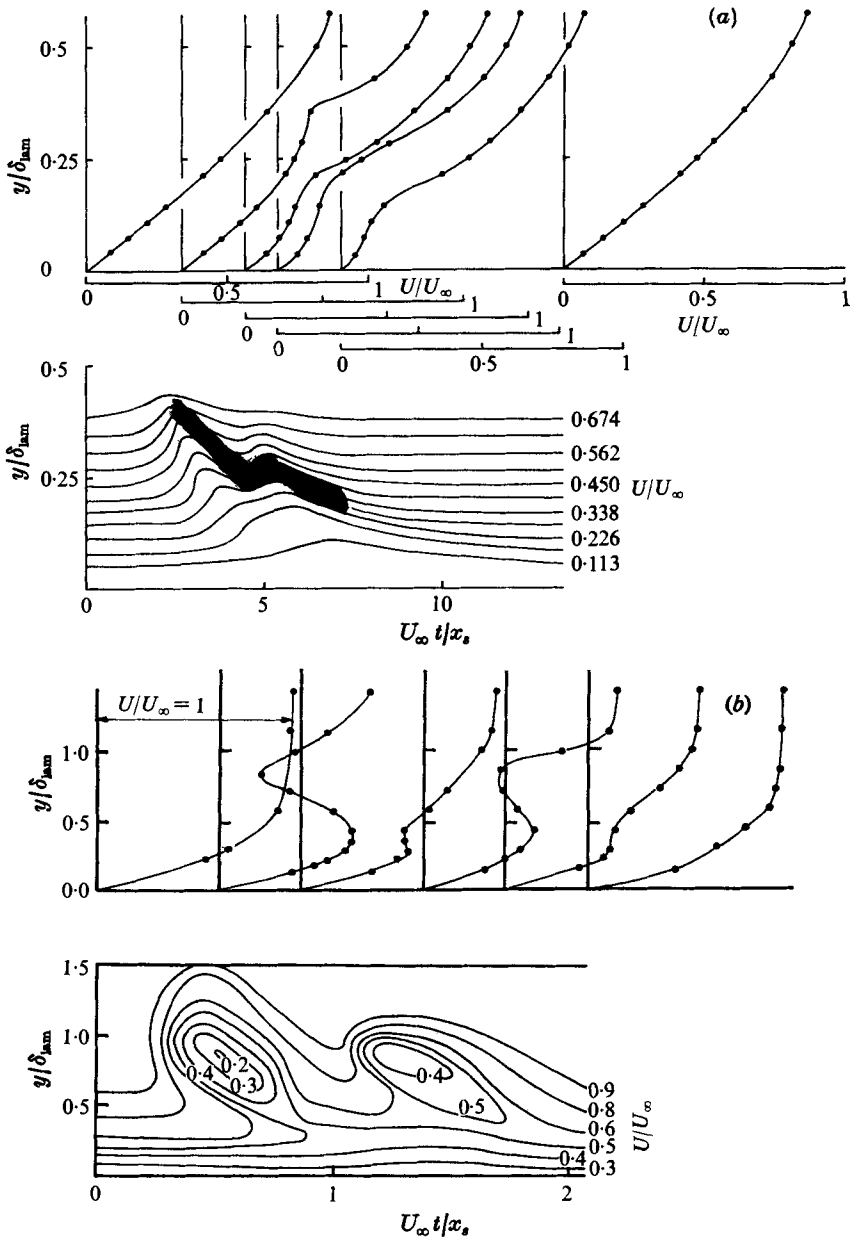

FIGURES 13 (*a*, *b*). For legend see facing page.

interface corresponds initially to the thickness of the laminar boundary layer, but once the spot has developed the surrounding boundary layer seems to have little or no effect on its shape. The laminar boundary layer does, however, affect the rate of growth of the spot. A dashed line showing the thickness of a hypothetical turbulent boundary layer originating at the spark with initial thickness equal to that of the laminar boundary layer at that location is also shown in the figure; it corresponds approximately to the maximum height of the spot. It is

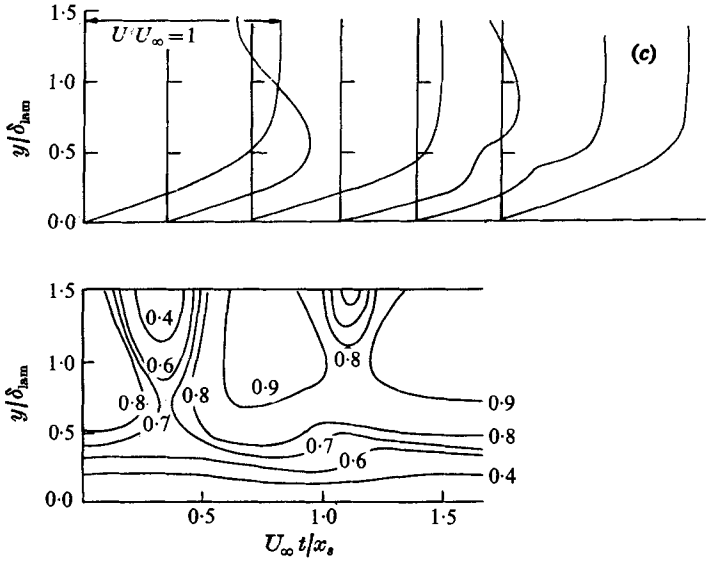

FIGURE 13. The flow field in the vicinity of various disturbances, $z = 0$.

	x_s/δ_{lam}	U_∞ (m/s)	x_{spark} (cm)
(*a*)	1·5	9·4	120
(*b*)	8·14	—	30
(*c*)	8·14	9·4	30

very difficult to say whether the top of the spot grows linearly with x_s (the distance from the spark) or as $x_s^{\frac{4}{5}}$ as may be inferred from the growth of a turbulent boundary layer. The average location of the top of the spot is hard to define, since all spots are not of equal height and since we rejected the points for which less than 50 % of the hot-wire signatures satisfied our criteria. A normalized elevation view of five different spots is drawn in figure 12. In order to make the comparison the length at the surface and the maximum height were taken as reference lengths. To show that the shape of the spot is independent of the disturbances which generated it, we changed the geometry of the spark and measured the velocities in its immediate neighbourhood. The ensemble averages in this case were related in time to the spark itself without additional realignment of the velocity spike. Three geometries were considered.

(*a*) A weak spark in the longitudinal direction along the surface of the plate 120 cm from its leading edge. This spark was so weak that at times it did not generate a turbulent spot (figure 13*a*).

(*b*) A strong spark skipping between two tiny protrusions in the spanwise direction a distance of 30 cm from the leading edge (figure 13*b*).

(*c*) A spark which was made to jump to the plate from a fine needle 3 cm long and placed 2 cm from the surface (figure 13*c*).

The disturbance in velocity which leads to the creation of the spot is different in each case, as may be seen from the velocity contours and corresponding velocity profiles. In case (*a*), $\partial u/\partial y$ is positive everywhere; in case (*b*), $\partial u/\partial y$ becomes negative twice between $0{\cdot}8 > y/\delta_{lam} > 0{\cdot}5$; in case (*c*), $\partial u/\partial y$ again becomes negative but at much larger distances from the surface than in case (*b*).

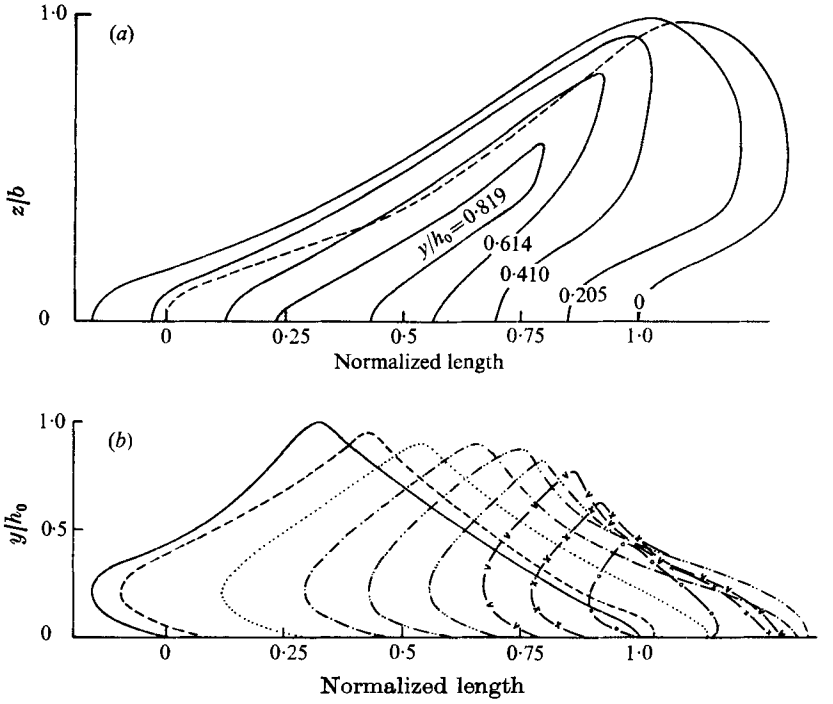

FIGURE 14. The shape of a 'typical' spot. (*a*) Contour map; $b/x_s = 0{\cdot}18$. (*b*) Cross-sections at various z/b; $h_0/x_s = 0{\cdot}025$. —, $z/b = 0$; – – –, $z/b = 0.118$; · · · · ·, $z/b = 0{\cdot}235$; —·—, $z/b = 0{\cdot}353$; —· · —, $z/b = 0{\cdot}471$; —· · · —, $z/b = 0{\cdot}588$; —v—, $z/b = 0{\cdot}706$; —x—, $z/b = 0{\cdot}824$; —o—, $z/b = 0{\cdot}941$.

The shear in this case is also less concentrated. An eventual deceleration of the flow near the plate and hence some ejection of fluid away from the surface is common to all three cases. This feature was also observed by Kovasznay *et al.* (1962) in their study of laminar boundary-layer breakdown, which was initiated by a vibrating ribbon above a flat plate on which strips of adhesive tape were pasted at regular intervals. All three types of disturbance lead to the creation of identical turbulent spots. It is thus tentatively concluded that the spot has a universal shape which is independent of the medium (Coles & Barker produced their spot in water), the Reynolds number (see also Elder 1962) and the way in which it was initiated.

A contour map of a 'typical' spot and a number of elevation views at various spanwise locations is shown in figures 14(*a*) and (*b*). The projection of the spot on the surface has an arrowhead shape with the leading interface slightly concave. The somewhat concave shape of the leading interface stems from the fact that U_{LE} decreases in the spanwise direction until it approaches U_{TE} at the edge of the spot. The contour map of the spot bears a remarkable resemblance to the contours of the maximum values of $\partial u/\partial y$ in the one spike stage of the breakdown of a laminar boundary layer (figure 11 of Kovasznay *et al.* 1962).

The maximum span of the spot near the surface is shown as a function of the distance from the disturbance and the free-stream velocity in figure 15. The spot grows linearly with downstream distance. The wedge angle, which repre-

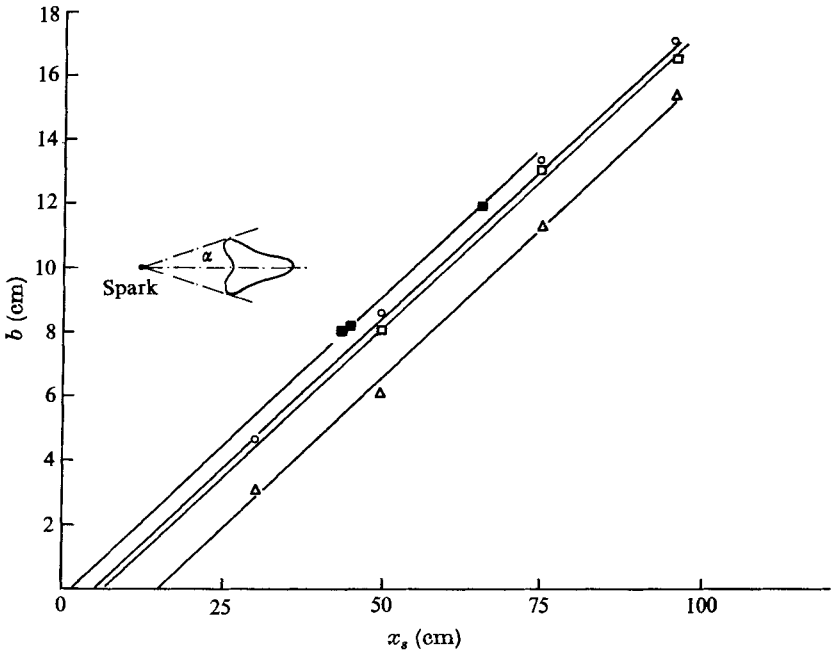

FIGURE 15. The spanwise growth of a spot at different Reynolds numbers.

	○	□	△	■
x_{spark}	30	30	30	120
U_∞ (m/s)	9·4	8	6	9·4
Re_{δ^*}(at spark)	508	468	406	1220

sents the spanwise growth of the spot, is approximately equal to 10°, irrespective of the location of the disturbance and the free-stream velocity. The hypothetical origin of the spot is usually downstream of the spark, implying that it takes some time for the spot to develop; this time becomes shorter with increasing Re. When the spark was located 30 cm from the leading edge of the plate the hypothetical origin of the spot was at a position corresponding to $Re_{\delta^*} = 530$ for the three velocities considered. This result is in good agreement with the measurement of S & K and does not conflict with stability theory, which predicts $Re_{\delta^*} = 450$ as the critical value below which all small disturbances should decay. When the spark was located 120 cm from the leading edge of the plate ($Re_{\delta^*} = 1220$), the hypothetical origin of the growth envelope of the spot was just 2 cm downstream; however the spread angle α remained unchanged. The rate of the elongation of the spot along the plane of symmetry may be obtained from the difference between the convection velocities of the interfaces: $dL/dt = U_{LE} - U_{TE}$. The time required for the spot to reach a probe located at a distance x_s downstream of the disturbance is $t = x_s/U_{LE}$ and the length of the spot at that location is $L = U_{TE}\,\Delta t$, where Δt is the duration of the spot signature. Since all these quantities are known one could, in principle, check the consistency of the data from the equation

$$\Delta t = \frac{U_{LE} - U_{TE}}{U_{LE}\,U_{TE}}\,x_s.$$

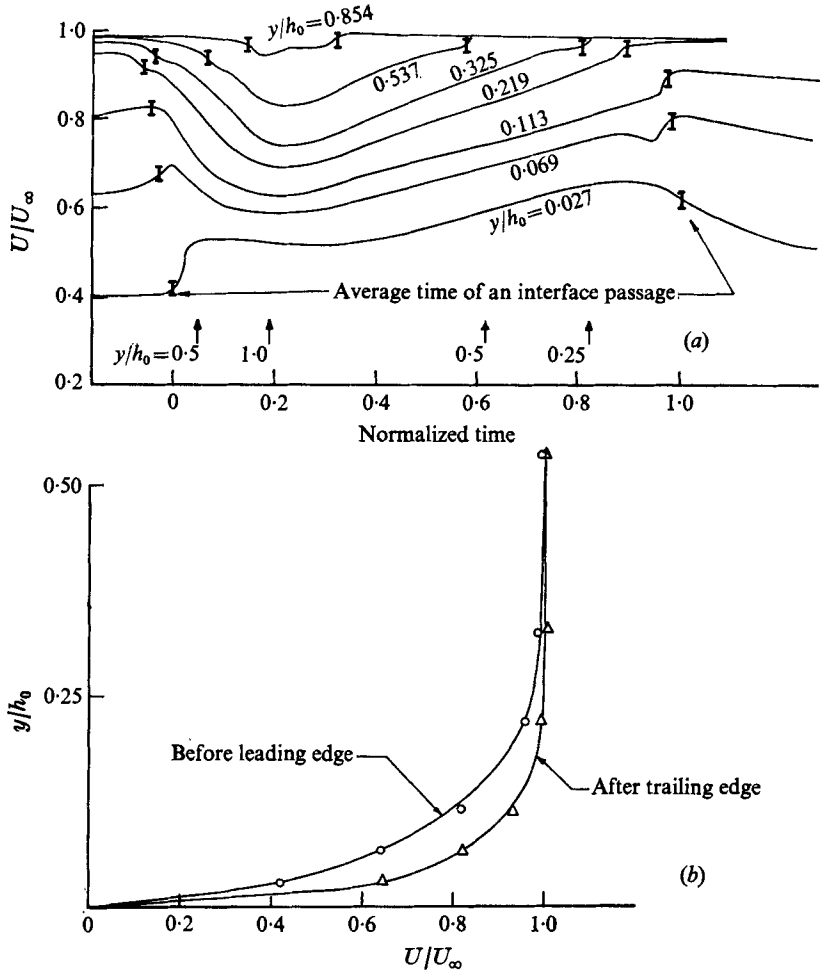

FIGURE 16. (*a*) A temporal record of velocities *in the plane of symmetry* at various distances from the plate. $U_\infty = 9{\cdot}4$ m/s, $h_0/x_s = 0{\cdot}02$, $x_s = 100$ cm, $z/b = 0$. (*b*) A comparison of two velocity profiles one upstream and the other downstream of the spot.

An equation of this sort is only valid for comparison of similar spots. It should not be used to predict the intermittency factor downstream of a line of stationary disturbances because the spots travel quite a long way before attaining similarity.

The mean flow field in a turbulent spot

A typical average temporal record of velocities at various distances y from the plate on the plane of symmetry ($z = 0$) is shown in figure 16(*a*). The distance from the plate is normalized by the maximum height h_0 of the spot, which was chosen as the most representative length scale despite the fact that it can not be measured with precision. The abscissa is normalized by the duration of the spot at the surface. The arrows shown at the bottom of the figure indicate the time at which the average height of the spot is the indicated fraction of h_0 (see also figure 18). As described earlier each curve was ensemble averaged twice, once conditioned to the leading interface and once conditioned to the trailing

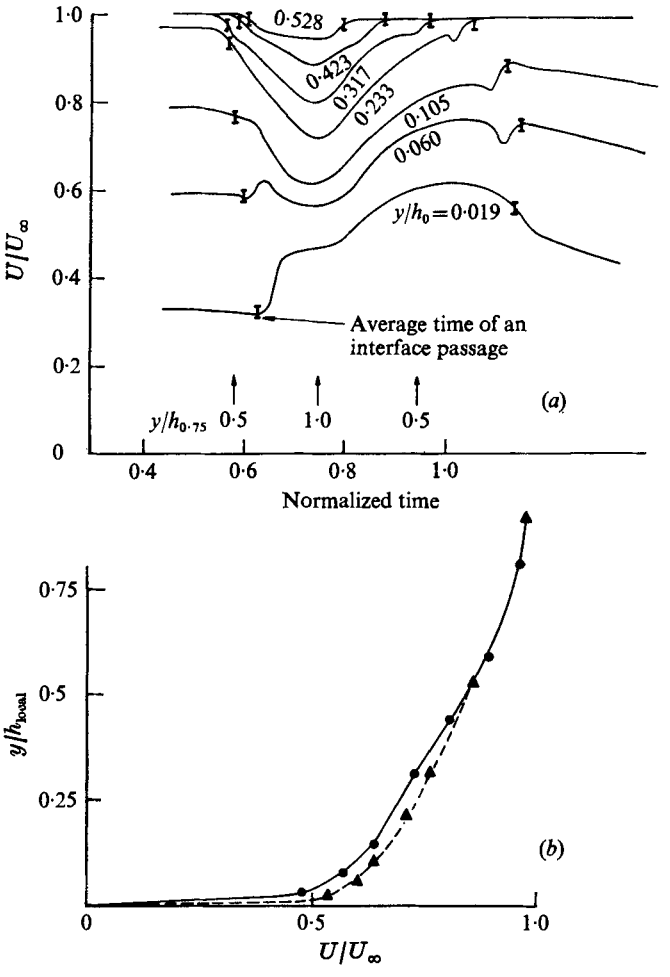

FIGURE 17. (*a*) A temporal record of velocities at various distances from the plate at $z/b = 0{\cdot}75$; $U_\infty = 9{\cdot}4$ m/s, $x_s = 100$ cm, $h_{0\cdot75}/h_0 = 0{\cdot}716$. (*b*) A comparison of two velocity profiles. ▲, $z/b = 0$, $x/x_{surface} = 0{\cdot}37$; ●, $z/b = 0{\cdot}75$, $x/x_{surface} = 0{\cdot}88$ (see figure 14*b*).

interface (see § 3). The two averages are identical over a period of time in the interior of the spot, thus they were easily matched. The velocity gradients become more moderate if one conditions the sampling to the disturbance generator; some detailed structure is then lost.

The velocity curves at different values of y were aligned to represent the time history which would have been recorded by a rake of hot wires located at those distances from the wall. The average time of the interface passage is also shown on this figure. Near the surface the velocity increases abruptly as the leading interface passes the measuring station; for within a millisecond the velocity may increase by a factor of 2 with respect to the unperturbed laminar flow. The acceleration then ceases (even very close to the wall) until the peak of the spot passes the measuring point, and resumes gradually as the spot passes by. The maximum velocity is attained near the trailing interface, sometimes right

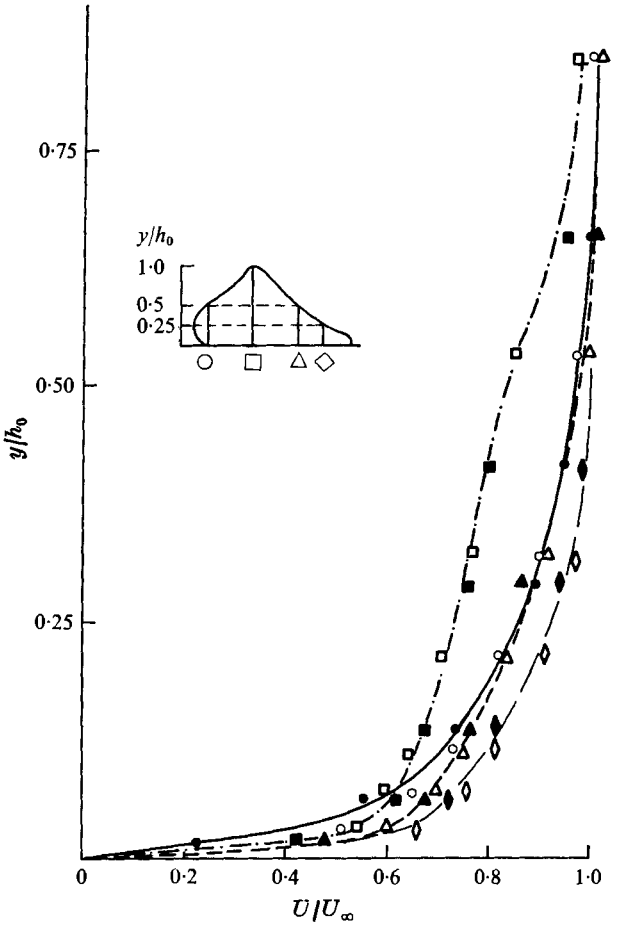

FIGURE 18. A comparison of velocity profiles in two different spots. Open symbols, $x_s = 100$ cm, $x_{spark} = 30$ cm; filled symbols, $x_s = 70$ cm, $x_{spark} = 120$ cm. $U_\infty = 9{\cdot}4$ m/s.

at the interface itself. Since the increase in velocity near the wall implies a steepening in the normal gradient $(\partial U/\partial y)_{y\to 0}$ the skin friction should increase accordingly. In the plane of symmetry, where the spanwise velocity vanishes ($W = 0$), the acceleration near the wall must be associated with an influx of fluid towards the surface. For $y/h_0 > 0{\cdot}1$ the flow decelerates as the spot arrives at the measuring station; the velocity attains a minimum under the peak of the spot and then increases slowly towards the trailing edge. The laminar velocity profile just downstream of the trailing edge is much fuller than the laminar profile upstream of the spot. While the profile in front of the spot resembles a Blasius profile for a laminar boundary layer in the absence of a pressure gradient, the profile downstream is fuller than the Falkner–Skan profile near a two-dimensional stagnation flow (figure 16*b*). The same pattern of flow can be observed at other locations along the span of the spot (i.e. $z \neq 0$), but since the spot is shorter and flatter there the variations in the average velocity records appear to be more pronounced (figure 17*a*). Because the cross-sectional shape

of the spot varies with span, one cannot expect the velocity profiles to collapse onto a single curve when scaled with the maximum height of the spot at a given spanwise location. Nevertheless such an attempt was made and its results are shown in figure 17 (*b*). The outer part of the profile at $z/b = 0{\cdot}75$ scales quite well with the local height while its inner part collapses onto the profile in the centre of the spot provided that it is scaled with the height h_0 at the centre. The comparison implies that for the average quantities the entire spot should be considered as one entity and one can not assume any spanwise independence, even though the variations in velocity along the span are much slower than the variations in the other two directions (x, y).

One may observe a sudden dip in the average velocity record near the trailing interface of the spot which is most apparent in the region $0{\cdot}05 < y/h_0 < 0{\cdot}3$ but does not appear in the immediate vicinity of the surface ($y/h_0 < 0{\cdot}03$). The dip represents a 'small' coherent eddy near the interface of the spot which was more pronounced in transitional pipe flow (Wygnanski *et al.* 1975). The acceleration following the dip appeared to be responsible in the case of the pipe flow for the splitting of turbulent puffs. We were unable to verify that splitting of turbulent spots indeed occurs because of the short distance (in terms of spot length) available for measurement; however, on some occasions it appeared that the spot might have split in two. Obviously more work is required to clarify this point, which may be an important feature of the transition process.

Measurements of velocity which were made in other spots show a remarkable similarity to the records shown in figure 16. Nevertheless a quantitative comparison is in order. In figure 18, four average velocity profiles which were measured in two spots of different size and origin are compared. The streamwise locations of the profiles are shown in the figure; they were arbitrarily picked to correspond to the locations at which the height of the spot is equal to, half of and a quarter of the maximum height respectively. The data points from both spots collapse onto the same curves. It may be concluded that *spots of similar shape also represent a similar velocity field.* We may now limit our discussion to a flow in a typical spot. The profiles indicate perhaps more clearly than before the high degree of order within the turbulent spot. Two points should be reiterated.

(i) $(\partial u/\partial y)_{y\to 0}$ increases towards the trailing edge of the spot.

(ii) The local thickness of the boundary layer (defined in the conventional way) follows approximately the height of the spot as long as the interface protrudes from the surrounding laminar boundary layer. For the most rearward profile drawn in figure 18 the local height of the spot is already within the laminar boundary layer and hence $\delta > \frac{1}{4}h_0$.

A plot of typical boundary-layer parameters – the displacement thickness δ^*, the momentum thickness θ and the shape factor $H = \delta^*/\theta$, which are shown in figure 19 – backs quantitatively some of the statements made. The displacement thickness increases rapidly downstream of the leading edge, attains a maximum where the spot's height peaks, and then decreases gradually towards the trailing edge. The displacement thickness is much less at the trailing edge than at the leading edge, i.e. $\delta^*_{LE}/\delta^*_{TE} \simeq 1{\cdot}75$. The momentum thickness behaves in a similar way, giving $\theta_{LE}/\theta_{TE} \simeq 2$. The distribution of θ follows the shape of the spot

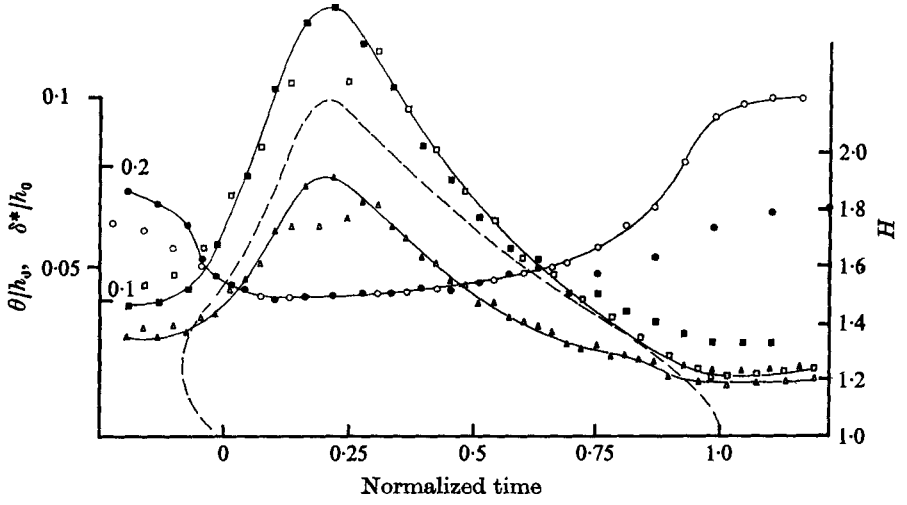

FIGURE 19. A histogram of δ^*, θ and H in the plane of symmetry of a spot. $x_s = 100$ cm, $U_\infty x_s/\nu = 1{\cdot}93 \times 10^5$. Open symbols, TE triggered; filled symbols, LE triggered. ○, H; △, δ^*; □, θ.

over 90 % of its total length; δ^* is less sensitive to the local thickness of the spot and starts to level off at $t = 0{\cdot}65$. The shape factor is almost constant within the turbulent region. The value of $H \simeq 1{\cdot}5$ is quite characteristic of a turbulent boundary layer at a low Re. At the trailing edge $H \simeq 2{\cdot}3$, which is approximately the value for stagnation-point flow. Downstream from the trailing edge H continues to increase, probably approaching 2·6, which is characteristic of a Blasius boundary layer. In front of the spot H decreases and is equal to 1·7 at the tip of the overhanging leading edge. The low value of H attained in a non-turbulent region indicates that some fluctuations are present in the flow upstream of the spot; these might have been partially communicated upstream by pressure waves which travel ahead of the spot. We did not investigate the 'calming-effect' discussed at length by S & K, but its existence is quite obvious from the boundary-layer parameters discussed.

The value of the dual interface ensemble-averaging procedure is well indicated by figure 19, in which the integral quantities for the boundary layer are presented. The correct H near the trailing interface is obviously the TE ensemble average and may be higher by 50 % than the value obtained from LE average data. It may be observed that the two ensemble averages agree well in the interior of the spot but diverge at opposite interfaces. At the maximum height of the spot there is again a discrepancy between LE-ensemble-averaged data and TE-ensemble-averaged data owing to the fact that the spot is very short near the peak and its variations in length there are relatively high.

The abscissa in figure 19 is normalized time rather than distance and hence the shape of the spot, which is shown for comparison, is distorted. This was done in order to prevent accumulation of possible errors by presenting data which are dependent on other measurements, namely U_{LE} and U_{TE}. The physical shape of the spot at $z = 0$ and the various flow parameters relating to it may be recon-

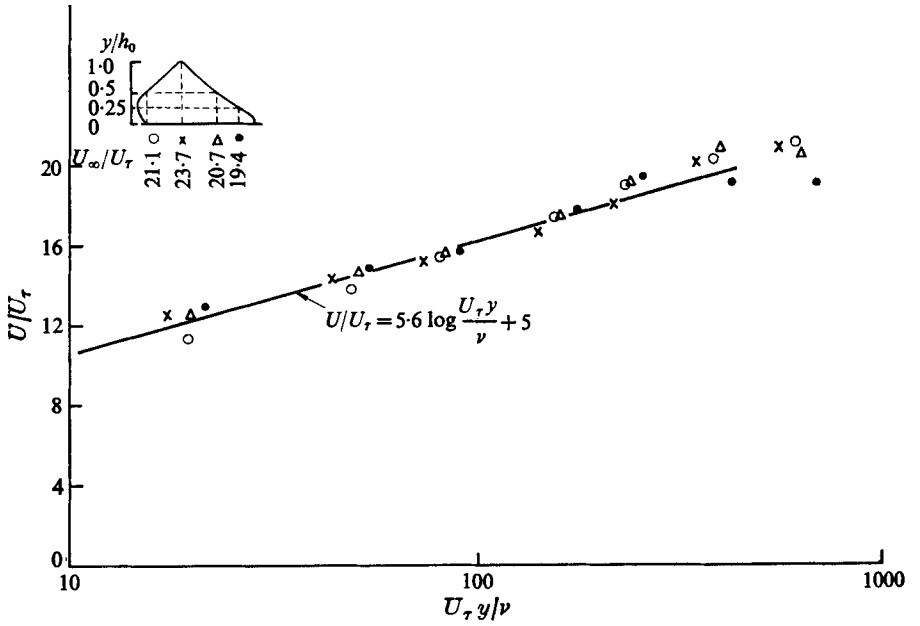

FIGURE 20. Some velocity profiles in a spot plotted in co-ordinates appropriate to the law of the wall.

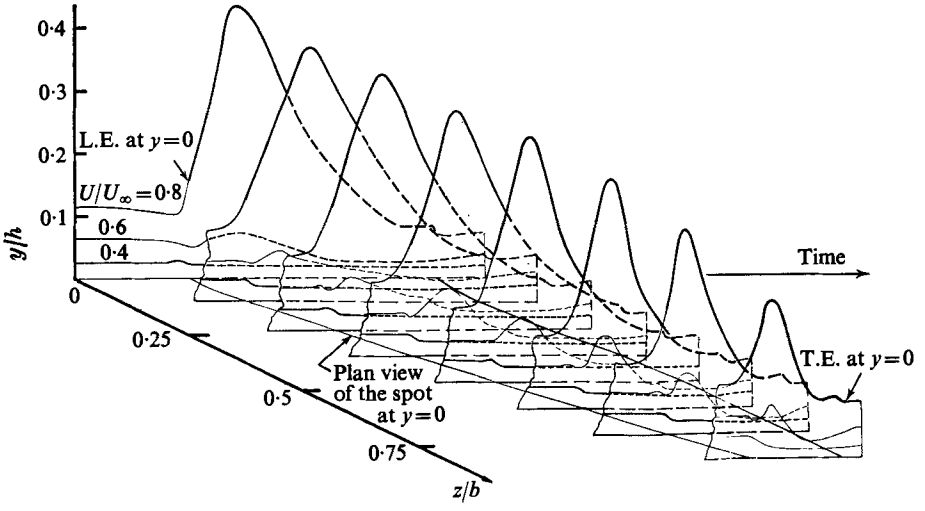

FIGURE 21. The spanwise distribution of those contours for which $U/U_\infty = 0{\cdot}8$, 0·6 and 0·4.

structed by stretching all data for which $t \leqslant 0{\cdot}2$ by a factor of 1·8, which is equivalent to the value of U_{LE}/U_{TE} at $z = 0$.

A logarithmic velocity distribution near the surface (the law of the wall) becomes a criterion for recognizing 'typical' boundary-layer flows at high *Re*. We replotted the four profiles in figure 20 in the appropriate wall co-ordinates and found that the logarithmic distribution represents the flow in a spot very

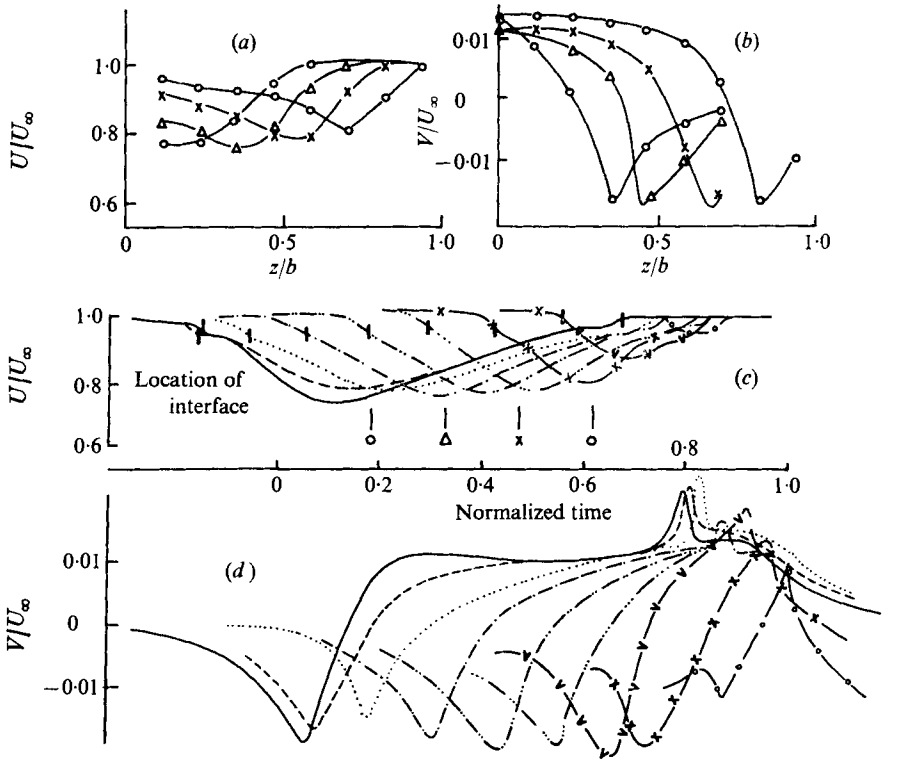

FIGURE 22. The spanwise variation of U and V at $y/h_0 = 0{\cdot}325$; $x_s U_\infty/\nu = 1{\cdot}93 \times 10^5$. ——, $z/b = 0$; – – –, $z/b = 0{\cdot}118$; · · · ·, $z/b = 0{\cdot}235$; —·—, $z/b = 0{\cdot}353$; —· · —, $z/b = 0{\cdot}471$; —· · · —, $z/b = 0{\cdot}588$; —v—, $z/b = 0{\cdot}706$; —x—, $z/b = 0{\cdot}824$; —o—, $z/b = 0{\cdot}941$.

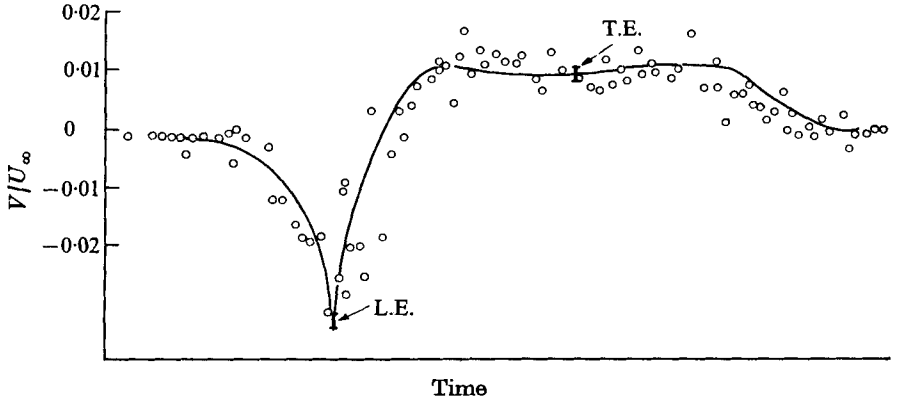

FIGURE 23. A comparison between measured and calculated normal velocity at $y/h_0 = 0{\cdot}54$ and $z/b = 0$; $U_\infty x_s/\nu = 1{\cdot}93 \times 10^5$. ○, computed; ——, measured.

well. The spot thus satisfies an important criterion common to turbulent boundary layers, and at first glance it would appear that we were dealing with a conventional boundary layer rather than with a well-defined turbulent structure. This test, however, is too superficial since a logarithmic profile represents little more than a local relationship between the skin-friction and velocity distribution. It is well known that the constants in this relation are independent of the pressure gradient, and hence to a large extent of upstream history. It is thus unreasonable to expect that they will contain any useful information about the sequence of events occurring in a spot. It is obvious from figure 20 that the second similarity criterion for turbulent boundary layers (the law of the wake) does not apply in the present case. The failure of the spot to conform with the defect law may be due in part to its low Re, but it may also imply that in contrast to boundary layers only a single scale governs the flow in the spot.

Because the spot is three-dimensional it is very difficult to represent the details of the flow field within it without resorting to a prohibitive number of graphs or tables, and even then one runs the risk of losing the general picture. It was therefore decided to cram some salient features of the flow into a small number of complicated figures. In figure 21, three contours of velocity for which $U/U_\infty = 0{\cdot}8$, $0{\cdot}6$ and $0{\cdot}4$ are plotted against time at various spanwise locations in the spot. The plot is presented as an isometric view, which represents well the coherence of the motion. The plan view of the spot at the surface is shown by the shaded area. The contours with $I/U_\infty = 0{\cdot}8$ diverge from the surface, following approximately the ridge-line of the spot at all values of z. The contours with $U/U_\infty = 0{\cdot}6$, which are initially much closer to the surface, also diverge from the plate but not nearly as much as those with $U/U_\infty = 0{\cdot}8$. The divergence of the second family of contours ($U/U_\infty = 0{\cdot}6$) from the wall is more pronounced at $z/b \geqslant 0{\cdot}35$ than at the plane of symmetry. The third family of contours ($U/U_\infty = 0{\cdot}4$) makes a step-like jump towards the surface of the plate. The net effect is an increased spread among the velocity contours under the ridge-line of the spot except in the immediate neighbourhood of the surface, implying that spanwise vorticity is removed from the outer part of the boundary layer and concentrated in the immediate vicinity of the wall. The coherence of the process in the z direction implies the existence of a single large structure which dominates the flow in the spot.

A horizontal traverse was taken across the spot at $y/h_0 = 0{\cdot}325$, all three components of velocity being drawn at different spanwise locations. In figure 22(*c*) each curve represents the time history of U as if it were measured by a horizontal rake of nine hot wires. The location of the interface is marked on each curve; the four marks at bottom of the figure indicate the times picked to show the variation of U with z (figure 22*a*). The locus of points at which U is a minimum moves outwards (in the direction of increasing z) as one proceeds towards the rear of the spot. By the time the minimum velocity is at $z/b > 0{\cdot}75$ the velocity at $z/b = 0$ has returned almost to its undisturbed level despite the fact that the entire section is still within the turbulent region.

The normal component of velocity V is strongly negative (i.e. towards the surface) near the leading interface, becoming positive throughout the rest of the

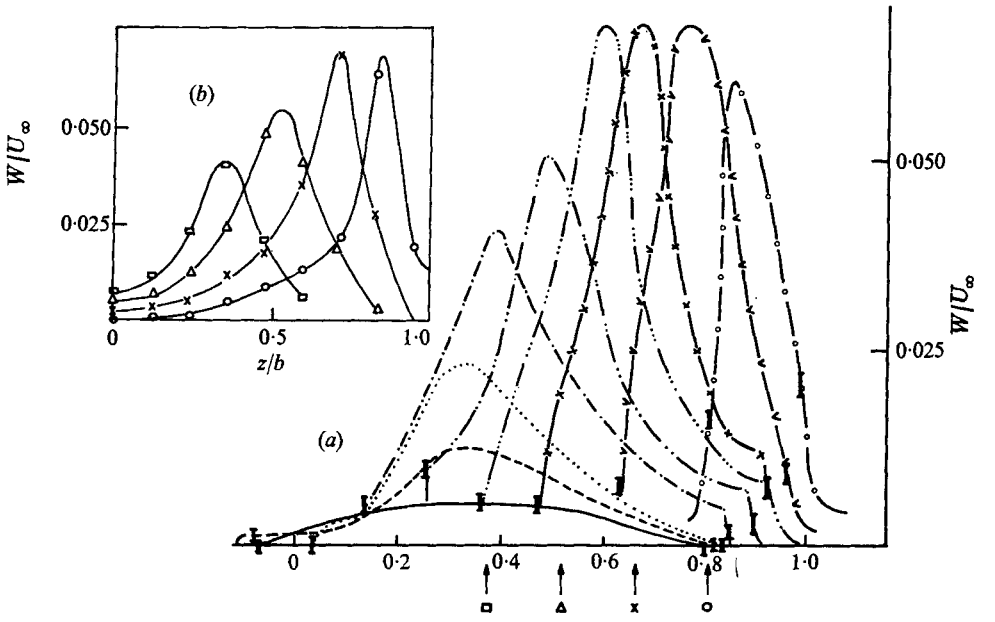

FIGURE 24. The spanwise variation of W at $y/h_0 = 0{\cdot}325$. —x—, $z/b = 0{\cdot}706$; —v—, $z/b = 0{\cdot}824$. Other curves as in figure 22.

spot with a sharply positive fluctuation near the trailing interface (figure 22*d*). The histogram of V resembles the flow in a typical vortex having a core which rotates like a solid body at large distances from the plane of symmetry (see curves for $z/b = 0{\cdot}941$ and $0{\cdot}824$ in figure 22*d*). The spanwise location of the peak in the V signal near the local leading edge of the spot does not correspond to the spanwise location of the minimum U signal at the same time co-ordinate (figures 22*a*, *b*). The normal velocity in the downward direction increases with increasing distance from the plate and the location of the leading interface moves closer to the most negative dip in the V signal, irrespective of z. Because the entire variation in V is about $0{\cdot}02\,U_\infty$ the accuracy of the measurement is of necessity low. Indeed the entire set of curves shown in figure 22 (*d*) originally had a zero offset equal to $0{\cdot}02\,U_\infty$. It is impossible to say whether the constant offset is real, resulting from a finite V in a laminar boundary layer, or an error in measurement resulting from a mismatch in the wires or a misalignment of the probe. We calculated the distribution of V on the plane of symmetry from the 'raw' LE-ensembled-average data on U and compared it with the measured V, assuming that it vanishes outside the spot and that $(\partial W/\partial z)_{z=0} = 0$. The result of the calculation is shown in figure 23 for $y/h_0 = 0{\cdot}54$ and agrees surprisingly well with the measurement. The strong positive fluctuation near the trailing edge can not be seen in this figure because it appears only in the TE-ensemble-averaged results. The temporal record of W at different z positions is shown in figure 24. The spanwise velocity increases with increasing z, attaining a rather flat maximum at $z/b > 0{\cdot}7$ at which $W/U_\infty \simeq 0{\cdot}07$. The small but finite

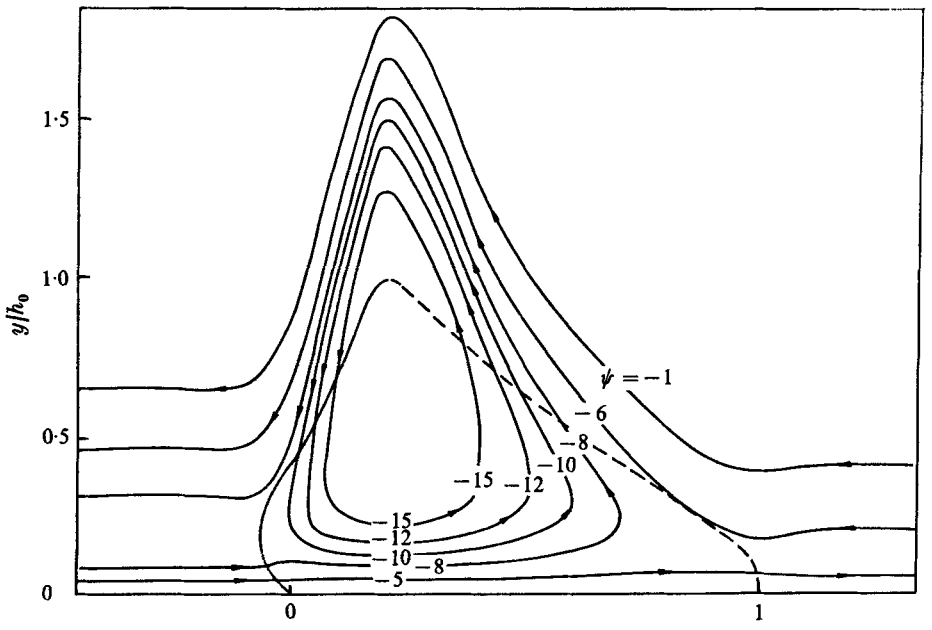

FIGURE 25. The streamlines relative to the leading interface of the spot. $U_\infty x_s/\nu = 1{\cdot}93 \times 10^5$, $z = 0$, $U_{LE}/U_\infty = 0{\cdot}9$.

value of W at $z = 0$ must be an error. It is possible that the probe was not perfectly aligned with the flow, or that the geometric centre-line on the plate did not coincide with the plane of symmetry of the spot in spite of the fact that preliminary measurements indicated that it did. An error which is equivalent to approximately 6 % of the maximum value of W is less than that anticipated. The distribution of W with time becomes steeper with increasing z (i.e. $\partial W/\partial t$ and hence $\partial W/\partial x$ increase with increasing z). A visual comparison with figure 22 (*d*) for $z/b > 0{\cdot}7$ indicates that W vanishes outside the core of the vortex. The variation of W with z at selected times (shown at the bottom of figure 24 *a*) is shown in figure 24 (*b*). On the basis of this figure one is justified in assuming that $(\partial W/\partial z)_{z=0} = 0$. The spanwise velocity at a given z increases with decreasing distance from the surface over most of the spot's cross-section, and it is everywhere directed outwards within the boundaries of the spot. The outward direction of W within the spot must surely be connected with its spanwise growth in the downstream direction.

The gross behaviour of the flow within the spot may be linked to tbe entrainment process. It appears, as in the flow in slugs in transitional pipe flow (Wygnanski & Champagne 1973), that there is a definite relationship between the velocity of the interface and the mean flow field by which relaminarization of the turbulent flow is prevented. This can be best shown by calculating the streamlines on the plane of symmetry in a frame moving with the respective interface. Such streamline patterns are shown in figures 25 and 26.

An extremely large eddy which extends in the y direction well beyond the

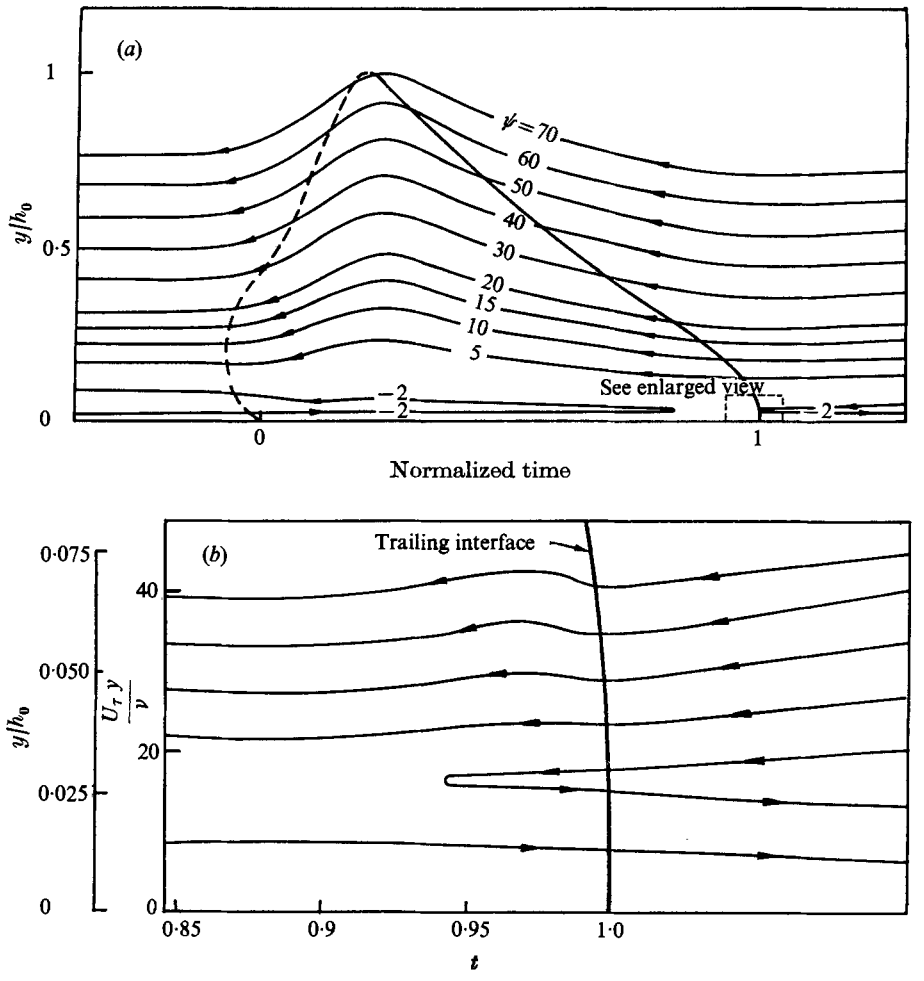

FIGURE 26. (*a*) The streamlines relative to the trailing interface of the spot. $U_\infty x_s/\nu = 1{\cdot}93 \times 10^5$, $z = 0$, $U_{TE}/U_\infty = 0{\cdot}5$. (*b*) Enlarged view of part of (*a*).

maximum height of the spot is seen in the frame of reference moving with the leading edge. All the streamlines penetrate the leading front and pass into the spot, indicating that no turbulent fluid escapes through this interface even though it moves slower than the free-stream velocity. This could not have been the case in the slug flow, where the propagation velocity of the leading interface must equal the maximum velocity in the pipe in order to prevent relaminarization. The difference stems from the fact that the spot has a finite height and the velocity just below the ridge is also less than U_∞.

The entrainment per unit length of the leading interface is most efficient near the surface and drops slowly with increasing y. Although the entire cross-section of the spot is outlined in figure 25, the trailing interface is marked by a broken line to stress the fact that the flow pattern does not apply to it.

The large eddy almost disappears when one considers the flow pattern relative to the trailing edge of the spot. Non-turbulent fluid is also entrained by the

trailing interface over most of its length. However, since the interface moves with a constant velocity independent of y, in the immediate vicinity of the wall it must overtake some fluid moving slower than U_{TE} owing to the no-slip condition at the surface. This would imply that relaminarization occurs near the wall. The process is most probably limited to the viscous sublayer (Wygnanski & Champagne 1973) because of the acceleration of the fluid which approaches the spot from behind. Thus the 'calming effect' which occurs behind a turbulent spot may be linked to the entrainment criterion for a turbulent/non-turbulent interface.

A detailed flow pattern in the wall region of the trailing interface is shown in figure 26 (*b*). There is a double ordinate in this figure, y/h_0 and $U_\tau y/\nu$, the second of which is not entirely independent of t since U_τ is not a constant (see figure 20). The variation of U_τ on this scale is small and it decreases towards the trailing edge. The figure helps to demonstrate that only a small amount of fluid from within the viscous sublayer manages to escape from the spot through the trailing interface. Thus the flow in the immediate vicinity of the interface and the surface resembles the flow in a slug (Wygnanski & Champagne 1973).

The spot as a large eddy

The streamlines which were drawn with respect to the leading interface (figure 25) give the impression that a single large vortex contains the entire spot. On the other hand, one needs to stretch one's imagination to see a large coherent structure when one looks at the streamline pattern relative to the trailing edge. It is obvious that what we see depends critically on the velocity of the reference frame in which we choose to observe the spot.

S & K assumed that the spot is convected with a velocity which is the arithmetic average of U_{LE} and U_{TE} (i.e. $U_c = 0{\cdot}5\,(U_{LE} + U_{TE}) = 0{\cdot}72\,U_\infty$). This assumption is justified because the spot retains its shape as it is convected downstream. Farabee *et al.* (1974) used the same assumption but obtained that $U_c = 0{\cdot}64\,U_\infty$ because they measured $U_{TE} = 0{\cdot}31\,U_\infty$. Coles & Barker (1974) tracked the locus of the minimum velocity in the spot and found a speed $U_c = 0{\cdot}83\,U_\infty$.

It was decided to resort to conventional statistical techniques, which are used in studying of turbulent flows, to resolve the question of the convection velocity. Two-point velocity correlations of each event were measured on the plane of symmetry of the spot ($z = 0$) in the vicinity of the surface ($y/h_0 = 0{\cdot}017$) and then ensemble averaged to give a smooth curve. The velocity signal near the wall is most suitable for this measurement since the trace of velocity *vs.* time resembles a square wave (figure 16*a*), resulting in a triangular correlation function (figure 27). The measurements were repeated for a different spanwise location ($z/b = 0{\cdot}75$) at two different distances from the wall. The wave form at this location has more of a triangular shape, giving rise to a parabolic correlation function. All points representing the time delay at which the correlation function attains a maximum for different distances (ΔX) between the measuring stations fell on a single straight line irrespective of ΔX (figure 28). The convection velocity for the entire spot was thus determined ($U_c = 0{\cdot}65\,U_\infty$).

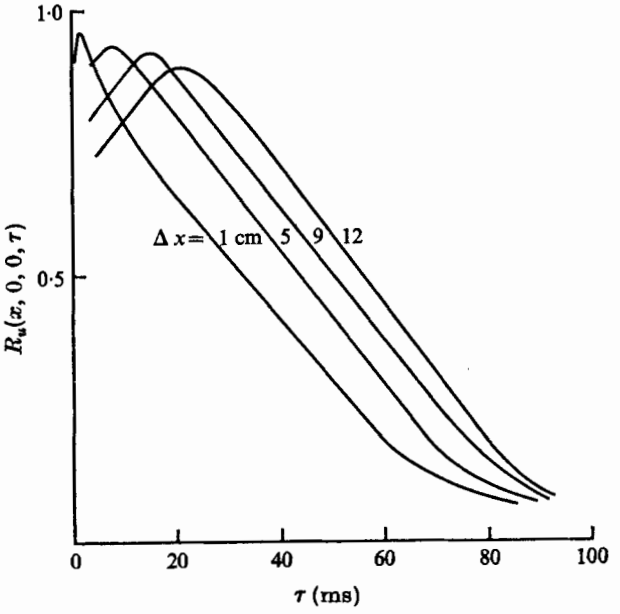

FIGURE 27. Two-point velocity correlations $R_u(x, 0, 0, \tau)$ on the plane of symmetry of the spot. $y/h_0 = 0{\cdot}017$, $x_s = 95$ cm, $U_\infty x_s/\nu = 1{\cdot}93 \times 10^5$.

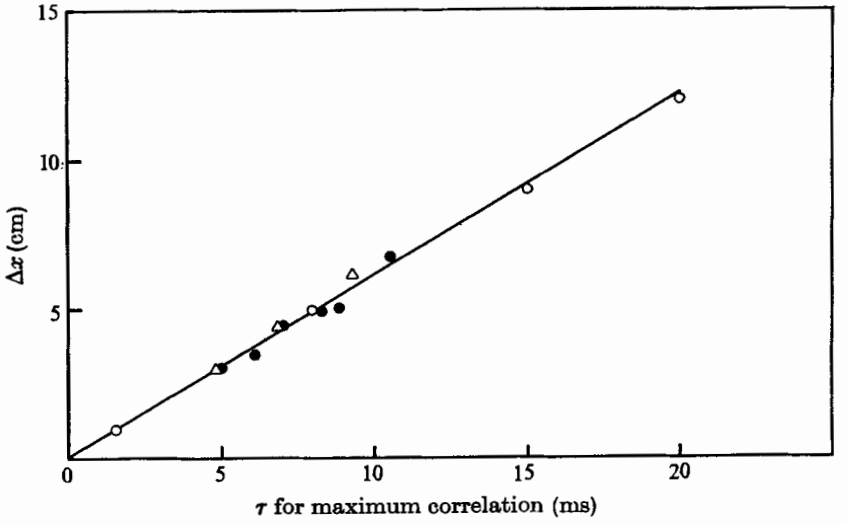

FIGURE 28. The locus of points for which the correlations are a maximum as a function of time delay. ○, $z/x_s = 0$, $y/x_s = 4{\cdot}44 \times 10^{-4}$; △, $z/x_s = 0{\cdot}133$, $y/x_s = 4{\cdot}22 \times 10^{-4}$; ●, $z/x_s = 0{\cdot}133$, $y/x_s = 4{\cdot}44 \times 10^{-4}$. $x_s = 90$ cm, $U_c/U_\infty = 0{\cdot}65$.

The difference between the two convection velocities ($U_c = 0{\cdot}83\,U_\infty$ and $U_c = 0{\cdot}65\,U_\infty$) was too large to be left unreconciled. It was suggested by Donald Coles that perhaps the value of U_c deduced from a two-point correlation is affected by the small-scale turbulence. The two signals were thus low-pass filtered prior to correlation. Nevertheless, the results did not change provided the cut-off frequency was higher than the frequency associated with the passage

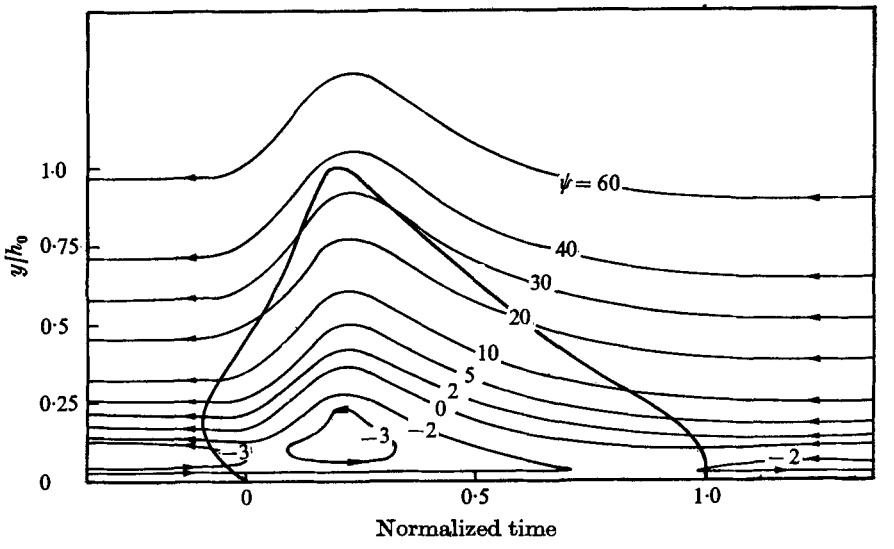

FIGURE 29. The streamline pattern in a reference frame convected with the spot. $U_c/U_\infty = 0{\cdot}65$, $U_\infty x_s/\nu = 1{\cdot}93 \times 10^5$, $z = 0$, $x_s = 100$.

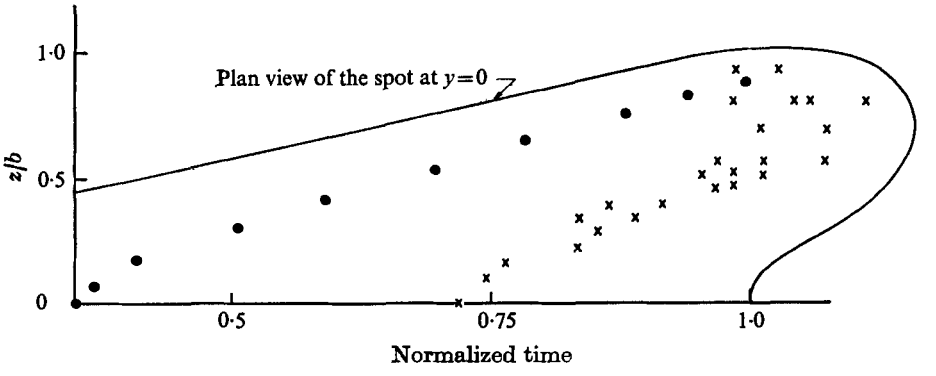

FIGURE 30. The spanwise variation of the locus of points for which the U correlation is a maximum. $U_\infty = 9{\cdot}4$ m/s. ●, $y/h_0 = 0{\cdot}21$; ×, $y/h_0 = 0{\cdot}017$.

of the spot. Tracking the locus of minimum velocity at a constant distance from the surface indeed produces an apparent speed $U_c = 0{\cdot}83\,U_\infty$. The result is apparent because the comparison is not made at the same geometrical location in the spot. When due care was taken to account for the growth of the spot with downstream distance the locus of the minimum velocity was convected at $U_c = 0{\cdot}64\,U_\infty$.

The streamline pattern in a reference frame moving with the spot is shown in figure 29. The closed loop given by $\psi = -3$ represents the core of the large eddy. On average the fluid within the core has no way to escape as long as the spot retains its shape. Although the size of the closed loop represents no more than 20% of the size of the spot its shape is remarkably similar to the shape of the spot. As the spot grows while moving downstream we expect the core to

grow proportionally. It may do so by wrapping around itself additional streamlines like the line $\psi = -2$, which is almost wrapped around the core already. No conclusion should be drawn from figure 29 about the mechanism by which the boundaries of the spot entrain laminar fluid.

The plan view of the core of the large eddy can in principle be obtained from two-point velocity correlations in the z direction. The variation in time delay necessary to maximize the correlation of velocity between two measuring stations separated by a distance Δz is shown in figure 30. The correlations were initially measured with the two wires very close to the surface ($y/h_0 = 0{\cdot}017$). The resulting correlation functions were quite flat and it was difficult to determine where the point of maximum correlation lies. The results deteriorated with increasing Δz as may be observed from the shaded area in the figure. It was later realized that the uncertainty in the data was inherent in the measurement, because we were essentially correlating two wave forms each resembling a square wave of a different duration. The correlation function, being ideally a trapezoid, does not have an identifiable maximum. The measurements were repeated at $y/h_0 = 0{\cdot}21$, and the time delay required to maximize the correlations in the z direction is plotted in the figure together with the plan view of the spot in the t, y, z co-ordinate system. The locus of these points describes a line which is almost parallel to the leading interface and coincides approximately with the ridge-line of the spot. From these measurements and the measurements of the velocity field one may conclude that the spot is a large vortex tube having an arrowhead shape. Near the plane of symmetry the vorticity is concentrated near the leading and trailing interfaces (see figure 22*d*) with a region of lesser activity in the centre. As the vortex tube narrows with increasing z the inactive region disappears and a well-defined spanwise vortex emerges. The core of the vortex appears to rotate in a manner resembling solid-body rotation. The fluid in the core acquires a spanwise component of velocity in the z direction.

Fluid deep in the laminar boundary layer overtakes the rear interface of the spot, and is entrained into it. Some fluid outside the laminar boundary layer but adjacent to it passes above the ridge of the spot and is entrained through the leading interface. The vortical motion created this way is probably responsible for the creation of a low pressure region in the centre of the spot with a favourable pressure gradient in the z direction which draws the fluid from the plane of symmetry to the outer edges of the spot. The resulting flow in the core accelerates in z direction. This description differs slightly from the U-shaped vortex which was previously ascribed to the turbulent spot.

It is very tempting to compare the flow pattern in a turbulent spot to the visual observations made by Offen & Kline (1974) in a turbulent boundary layer. If a spot were to move past dye injectors of the type described by Offen & Kline they would most probably report a 'sweep' (which brings in fluid from the outer part of the boundary layer towards the wall) followed by a 'burst' in which some dye would have been ejected from the wall outwards. The different duration of 'sweeps' and 'bursts' can be attributed to the fact that naturally created spots arrive at the measuring station from different locations in x and z. We thus may be observing spots which are at different stages of their develop-

ment and at different spanwise locations. Furthermore we do not know how adjacent spots interact and whether they produce new spot-like structures in the process.

In conclusion, the comparison between the two phenomena is very attractive and it remains to be seen whether a spot which is artificially produced in a laminar boundary-layer transition region can be detected and followed in a turbulent boundary layer.

This research was sponsored by the Airforce Office of Scientific Research, Office of Aerospace Research United States Airforce, Grant AFOSR-72-2346, and monitored by Major Daniel R. Seger, E.O.R.

REFERENCES

BETCHOV, R. & CRIMINALE, W. O. 1967 *Stability of Parallel Flows*. Academic.

COLES, D. & BARKER, S. J. 1974 *Proc. Purdue Workshop on Turbulent Mixing* (ed. S. N. B. Murthy), p. 285. Plenum.

DHAWAN, S. & NARASIMHA, R. 1958 *J. Fluid Mech.* **3**, 418.

ELDER, J. W. 1962 *J. Fluid Mech.* **9**, 235.

EMMONS, H. W. 1951 *J. Aero. Sci.* **18**, 490.

FARABEE, T. M., CASARELLA, M. J. & DEMETZ, F. C. 1974 *Naval Ship R. & D. Center Rep.* SAD-89E-1942.

KLEBANOFF, P. S., TIDSTROM, K. D. & SARGENT, L. M. 1962 *J. Fluid Mech.* **12**, 1.

KOVASZNAY, L. S. G., KOMODA, H. & VASUDEVA, B. R. 1962 *Proc. Heat Transfer & Fluid Mech. Inst.* Stanford University Press.

MORKOVIN, N. V. 1969 In *Viscous Drag Reduction* (ed. C. S. Wells), p. 1. Plenum.

OFFEN, G. R. & KLINE, S. J. 1974 *J. Fluid Mech.* **62**, 223.

SCHUBAUER, G. B. & KLEBANOFF, P. S. 1956 *N.A.C.A. Rep.* no. 1289.

TANI, I. 1969 *Rev. Fluid Mech.* **2**, 169.

WYGNANSKI, I. J. & CHAMPAGNE, F. H. 1973 *J. Fluid Mech.* **59**, 281.

WYGNANSKI, I. J., SOKOLOV, M. & FRIEDMAN, D. 1975 *J. Fluid Mech.* **69**, 283.